

Molecular and functional mechanisms of long-term visual habituation in larval zebrafish

Laurie-Anne Lamiré¹, Martin Haesemeyer², Florian Engert^{3,4†}, Michael Granato^{5†}, Owen Randlett^{1†,*}

*Correspondence:

owen.randlett@univ-lyon1.fr (OR)

†Equal contribution

¹ Laboratoire MeLiS, UCBL - CNRS UMR52684 - Inserm U1314, Institut NeuroMyoGène, Faculté de Médecine et de Pharmacie, 8 avenue Rockefeller, 69008, Lyon, France ; ² The Ohio State University, Department of Neuroscience, Columbus, OH 43210, USA ; ³ Department of Molecular and Cellular Biology, Faculty of Arts and Sciences, Harvard University, Cambridge, MA 02138, USA ; ⁴ Center for Brain Science, Faculty of Arts and Sciences, Harvard University, Cambridge, MA 02138, USA ; ⁵ Department of Cell and Developmental Biology, University of Pennsylvania, Perelman School of Medicine, 421 Curie Blvd, Philadelphia, PA 19104, USA

Abstract Long-term habituation allows animals to learn to ignore persistent but unimportant stimuli. Despite being the most basic form of learning, a consensus model on the underlying mechanisms has yet to emerge. We have exploited a visual habituation paradigm in larval zebrafish, where larvae will learn to reduce their reactions to abrupt global dimming (a dark flash). Using a drug-screening approach, we first identified pathways that potently altered habituation learning, including GABAergic inhibition, Melatonin and Estrogen signaling. To determine how habituation manifests at the circuit-level, we used whole-brain pERK and 2-photon Ca²⁺ imaging. These analyses identified 12 classes of neurons that differ in their stimulus response profile, rate of adaptation during learning, anatomical location, and GABAergic identity. By analyzing how GABA and Melatonin alter population activity, we propose a model for dark flash habituation in which the suppression of activity begins early in the visual pathway but downstream of the retina. This suppression is mediated by GABAergic inhibitory motifs resulting in heterogeneous inhibition of distinct neuronal types in the dark flash circuit. Our results have identified multiple molecular pathways acting in functional cell types underlying a form of long-term plasticity in a vertebrate brain, and allow us to propose the first iteration of a model for how and where this learning process is encoded in individual neurons to shape learned behaviour.

Introduction

A central function of the brain is to change with experience: learning from the past to adapt behaviours in the now. At a base level, these adaptations can reflect attempts to identify and attend preferentially to salient stimuli. For example, identifying the smell of a predator or prey may be crucial, while identifying that my home still smells like my kin is not. This ability to suppress responses to continuous stimuli is known as habituation, and is generally considered to be the simplest form of learning and memory *Rankin et al. (2009)*. Habituation is conserved across all animals, and like other forms of plasticity, exists in at least two mechanistically distinct forms: transient short-term habituation, and protein-synthesis dependent long-term habituation. Here we focus on long-term habituation, which serves as a pragmatic model to dissect the molecular and circuit mechanisms of stably encoded plasticity processes in neural circuits.

In recent years, a renewed focus on long-term habituation has led to significant insights into the adaptations underlying this process *Cooke and Ramaswami (2020); McDiarmid et al. (2019b)*, nonetheless a consensus model on the general principles underlying habituation is yet to emerge. Physiological and genetic work in *Aplysia*, and *C. elegans* were consistent with a model in which homosynaptic depression of excitatory synapses drives habituation *Bailey and Chen (1983); Rose et al. (2003)* (although see *Glanzman (2009)*). In contrast, recent work in the *Drosophila*

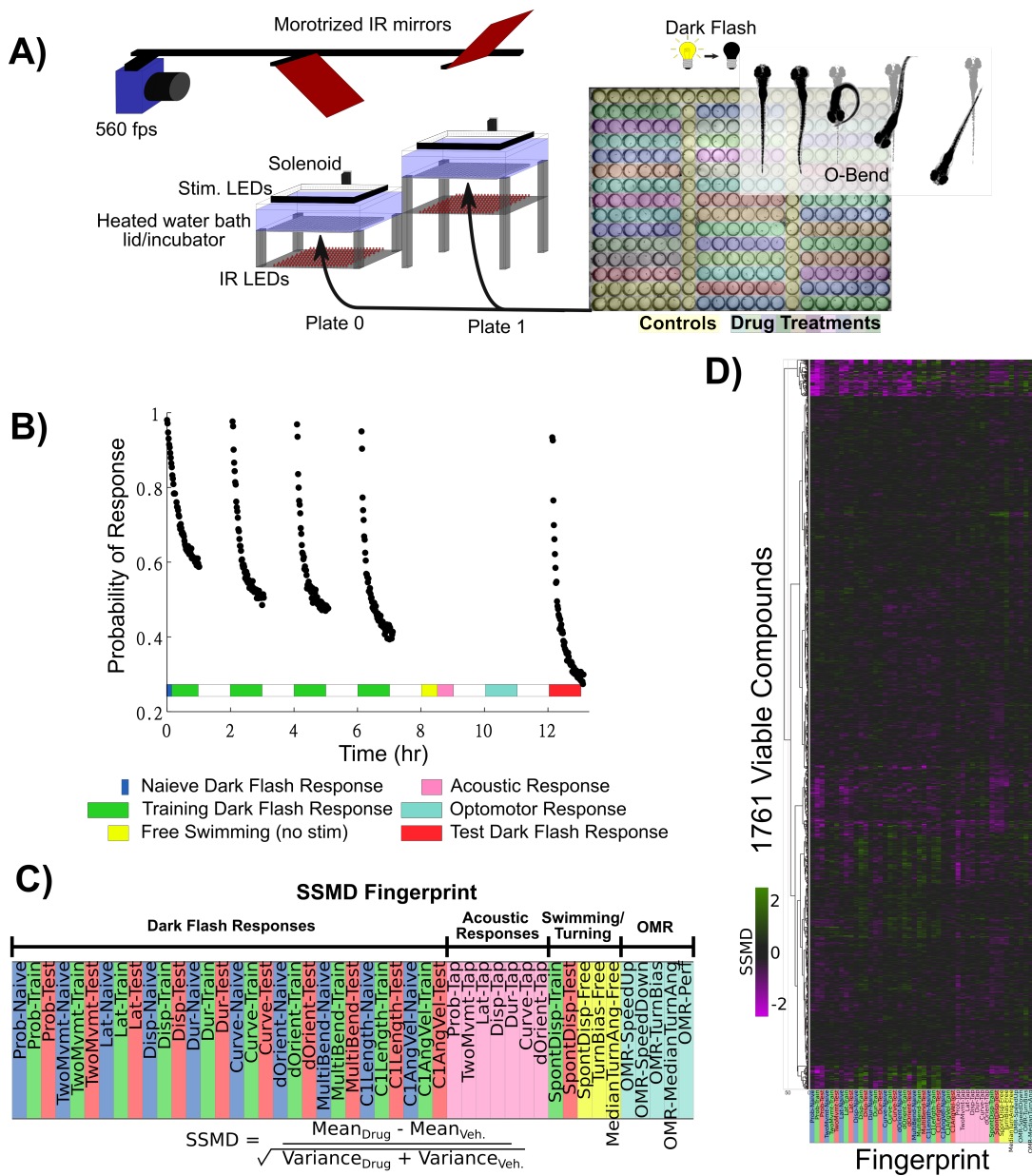


Figure 1. Pharmacological screening for dark flash habituation modulators.

A) Screening setup to record larval zebrafish behaviour in 300-well plates, which are placed below a 31°C water bath that acts as a heated lid for the behaviour plates. Two 300-well plates are imaged in alternation using mirrors mounted on stepper motors. Fish are illuminated with infra-red LEDs and imaged with a high-speed camera recording at 560 frames per second (fps). Visual stimuli are delivered by a rectangular ring of RGB LEDs, and acoustic stimuli are delivered via a solenoid mounted on the back of the water tank. Colors overlaid on the 300-well plate indicate the arrangement of small molecule treatments and controls (yellow).

B) Habituation results in a progressive decrease in responsiveness to dark flashes repeated at 1-minute intervals, delivered in 4 training blocks of 60 stimuli, separated by 1hr of rest (from 0:00-8:00). This epoch is separated into periods reflective of the Naive response (first 5 stimuli, blue), and the remaining 235 stimuli during Training (green). From 8:00-8:30, no stimuli are delivered and fish are monitored for spontaneous behaviour (yellow). From 8:30-9:00 fish are given acoustic stimuli via the solenoid tapping on the water bath (pink). From 10:00 - 11:00 fish are stimulated with alternating leftward and rightward motion using the RGB LEDs to induce the optomotor response and turning towards the direction of motion (light blue). Finally, at 12:00-13:00, larvae are given 60 additional dark flashes during the test period (red).

C) The strictly standardized mean difference (SSMD) is calculated across these different time periods, behaviours and the different components of O-Bend behavioural habituation (Randlett et al., 2019). All drugs were dosed at 10 µM in 0.1% DMSO ($n = 6$ larvae), relative to 0.1% DMSO vehicle controls ($n = 60$ larvae).

D) These vectors are assembled across all screened drugs that were viable and did not cause death or paralysis of the larvae. Displayed as a hierarchically clustered heatmap of behavioural Fingerprints (vectors of SSMD values). Clustering distance = ward, standardized euclidean.

Figure 1—source data 1. Small molecule library, Selleckchem Bioactive: 2100 FDA-approved/FDA-like small molecules

Figure 1—source data 2. Behavioural fingerprints for viable compounds

olfactory and gustatory systems indicate that the potentiation of inhibitory neurons drives habituation rather than depression of excitatory connections *Das et al. (2011); Paranjpe et al. (2012); Trisal et al. (2022)*, and habituation to specific orientations of visual cues in mice is associated with the potentiation of neuronal activity and synapses in the visual cortex *Cooke et al. (2015)*, which requires GABAergic interneurons *Kaplan et al. (2016)*. These studies are more consistent with a model in which the potentiation of inhibition, rather than depression of excitation, drives habituation *Cooke and Ramaswami (2020)*.

Recently, we found that long-term habituation of the response of larval zebrafish to sudden pulses of whole-field darkness, or dark flashes (DFs), involves multiple molecularly independent plasticity processes that act to suppress different components of the behavioural response *Randlett et al. (2019)*. Similar behavioural, pharmacological, and genetic experiments have led to comparable conclusions in acoustic short-term habituation *Nelson et al. (2022)*, and habituation in *C. elegans* *McDiarmid et al. (2019a,b)*, indicating that habituation generally acts via multiple modular plasticity processes. These modules act to mute or shift behavioural responses to repeated stimuli. How and where these processes are implemented in the circuit, and how conserved or derived these processes are across species or paradigms remains to be determined.

Here we have used a combination of high-throughput behavioural analyses, pharmacology and whole brain imaging to propose a model of DF habituation. By combining knowledge about critical neurotransmitters derived from pharmacology, with knowledge about functional classes of neurons derived from whole-brain imaging, we have established a model constrained on multiple scales.

Results

Pharmacological screening strategy

When stimulated with a dark flash (DF), larval zebrafish execute an O-bend response. The O-bend is characterised by a strong body bend and a large angle turning maneuver that forms part of the phototactic strategy of larval zebrafish, helping them navigate towards lit environments *Burgess and Granato (2007); Chen and Engert (2014)*. When trained with repeated DFs, larvae will habituate and reduce their responsiveness in multiple independent ways, including: decreasing response probability, increasing latency, and decreasing multiple measures of response magnitude *Randlett et al. (2019)*. As the molecular mechanisms leading to this form of habituation learning are still largely unknown, we used a pharmacological screening approach with the goal of identifying important molecular players in habituation. We used the high-throughput assay we previously established, which has a maximum throughput of 600 larvae/day (*Figure 1A, Randlett et al. (2019)*). As we aimed to identify modulators specific for habituation, we included additional behavioural assays as controls, including the response to acoustic stimuli, the optomotor response, and the spontaneous swimming behaviour of the fish in the absence of stimulation (*Figure 1B,C*).

Behavioural records for fish treated with each compound were compressed into a fingerprint *Rihel et al. (2010)* – a vector representing the strictly standardised mean difference (SSMD) across 47 aspects of behaviour (see Methods). For measurements related to dark-flash habituation behaviour, responses were time-averaged across three epochs chosen to highlight changes in habituation: the naive response (first 5 dark flashes), the response during the remaining training flashes, and the re-test block 5 hrs after training (*Figure 1B*). This was done across 10 different components of the dark flash response (Probability of Response, Latency, Displacement, etc.).

In each 300-well plate, 40 groups of 6 larvae were treated in individual wells, and compared to 60 vehicle treated controls (*Figure 1A*). We chose these numbers based on a sub-sampling analysis that determined these numbers were sufficient to identify the effect of a known modulator of habituation (haloperidol *Randlett et al. (2019)*) at a false-negative rate of less than 0.05 (not shown), while allowing us to screen 80 drugs per experiment across 2 plates (*Figure 1A*).

Correlational structure in the pharmaco-behavioural space

We screened a total of 1953 small molecule compounds for their acute effects on behaviour (*Figure 1-source data 1*)), focusing on both activators and inhibitors with annotated targets. We were able to collect the full behavioural record of 1761 compounds (*Figure 1D, Figure 1-source data 2*)), indicating that the fish survived the treatment and maintained their ability to swim. We found that 176 drugs significantly altered at least one aspect of measured behaviour, yielding a 9% hit rate (hit threshold of $|SSMD| \geq 2$). While the average effect was to suppress behavioural

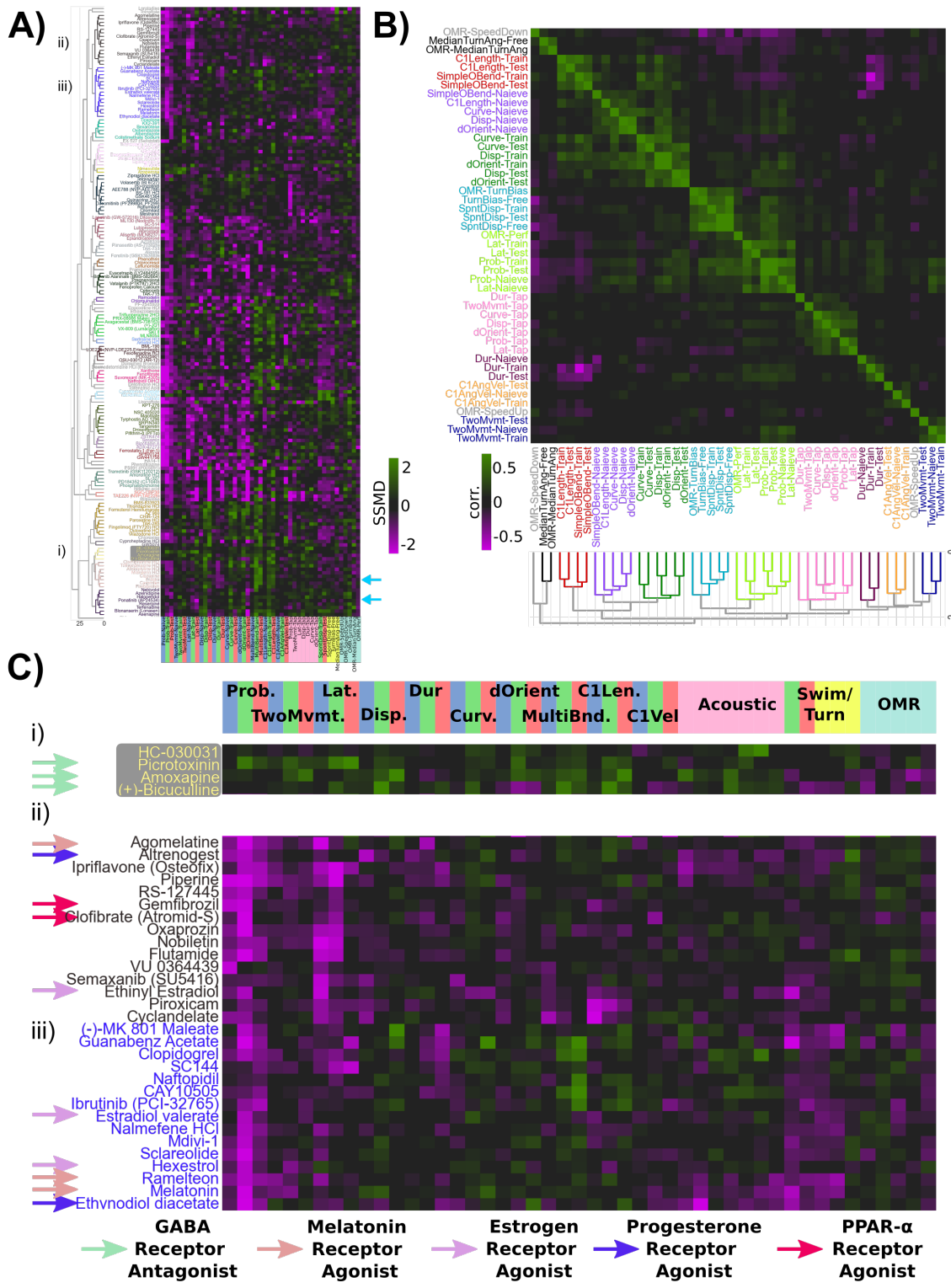


Figure 2. Pharmaco-behavioural analyses of behaviour-modifying compounds.

A) Clustered heatmap of the behavioural Fingerprints for the 176 hits of the screen, showing at least one behaviour measure with $|SSMD| \geq 2$. Clustering distance = ward, standardized euclidean. This led to the re-identification of Haloperidol and Clozapine as habituation modifiers (light blue arrows).

B) Clustered correlogram of the Pearson correlation coefficients for the different measured components of behaviour across hits (same data as (A)) revealing the independence or co-modulation of behaviours. Clustering distance = average, correlation.

C) Subsets of clustered heatmap from (A), highlighting the similar phenotypes exhibited by i) GABA Receptor antagonists and ii), iii) Melatonin receptor agonists, Estrogen receptor agonists, Progesterone receptor agonists and peroxisome proliferator-activated receptor alpha (PPAR α) agonists.

output ($SSMD = -0.20$), which could reflect non-specific toxicity or a generalized inhibition of motor output, the effect of most small molecules induced both positive and negative changes in behavioural output, indicating that toxicity is not the primary phenotypic driver (*Figure 2A*). While the false negative rate is difficult to determine since so little is known about the pharmacology of our system, we note that of the three small molecules we previously established to alter dark flash habituation that were included in the screen (Clozapine, Haloperidol and Pimozide), two were identified among our hits.

To explore the pharmaco-behavioural space in our dataset we clustered small molecules based on their behavioural phenotypes (*Figure 2A*). This strategy can identify drugs that share common pharmacological targets, or perhaps distinct pharmacological targets that result in convergent behavioural effects *Bruni et al. (2016); Rihel et al. (2010)*. Indeed, drugs known to target the same molecular pathways often showed similar behavioural fingerprints lying proximal on the linkage tree, indicating that our dataset contains sufficient signal-to-noise to recover consistent pharmaco-behaviour relationships.

Alternatively, drugs can be considered as tools to manipulate different aspects of brain function agnostic to their molecular mechanisms. Consequently, using similarities and differences among the induced alterations should uncover molecular and neural linkages among different behavioural outputs. Following this logic, the ability of a drug to co-modify different aspects of behaviour would reflect molecular and/or circuit-level dependencies. For example, visual behaviours that all depend upon the retinal photoreceptors should be similarly affected by any drugs that modulate phototransduction in these photoreceptors. We quantified these relationships by calculating the correlated effects on our different behavioural measurements across drugs (*Figure 2B*).

Consistent with our previous results highlighting uncorrelated learning across the behavioural components of the O-bend response during habituation *Randlett et al. (2019)*, we found that different aspects of the response were independently affected pharmacologically, resulting in distinctive correlated groupings within the correlogram. While we previously found that O-Bend response Probability and Latency habituate independently in individual fish *Randlett et al. (2019)*, in our drug screen data these appear to be tightly coupled (*Figure 2B*, green cluster). This may result from their reliance on a common molecular-level mechanism that occurs in distinct circuit loci. However, the performance of the animals in the OMR assay under different treatments was also associated with O-bend Probability and Latency, suggesting that pharmacological modulation of general visual acuity could drive these correlations within the drug screen dataset.

These analyses confirm habituation behaviour manifests from multiple distinct molecular mechanisms that independently modulate different behavioural outputs. Our screen was successful in identifying small molecules that differentially modulate these distinct aspects of habituation behaviour, as well as acoustic, optomotor, and spontaneous behaviour.

Molecular pathways implicated in habituation

For the remainder of the analyses we chose to focus on the mechanisms leading to the habituation of response probability, as this is the criterion for which it is easiest to identify the link between neural activity and behavior, providing the best entry point for studying the circuit mechanisms of long-term habituation. To identify the most promising hits, we sought to identify drugs that:

1. Have minimal effects on the naive response to DFs, but strong effects during the training and/or memory-retention periods. This would prioritize pathways that affect habituation, rather than simply DF responsiveness.
2. Have minimal effects on other aspects of behaviour. We purposefully assayed additional behaviours after habituation training in order to exclude compounds that would alter generalized arousal, movement ability/paralysis, or visual impairment. Such drugs would strongly influence DF responsiveness, but likely independently of pathways related to habituation.
3. Show similar behavioural effects to other drugs screened that target the same molecular pathway. Such relationships can be used to cross validate, yet we note that our library choice was very broad, and target coverage is non-uniform. Therefore a lack of multiple hits targeting the same pathway should not necessarily be taken as strong evidence of a false positive.

This prioritization led us first to the identification of the GABA_{A/C} Receptor antagonists Bicuculline, Amoxapine,

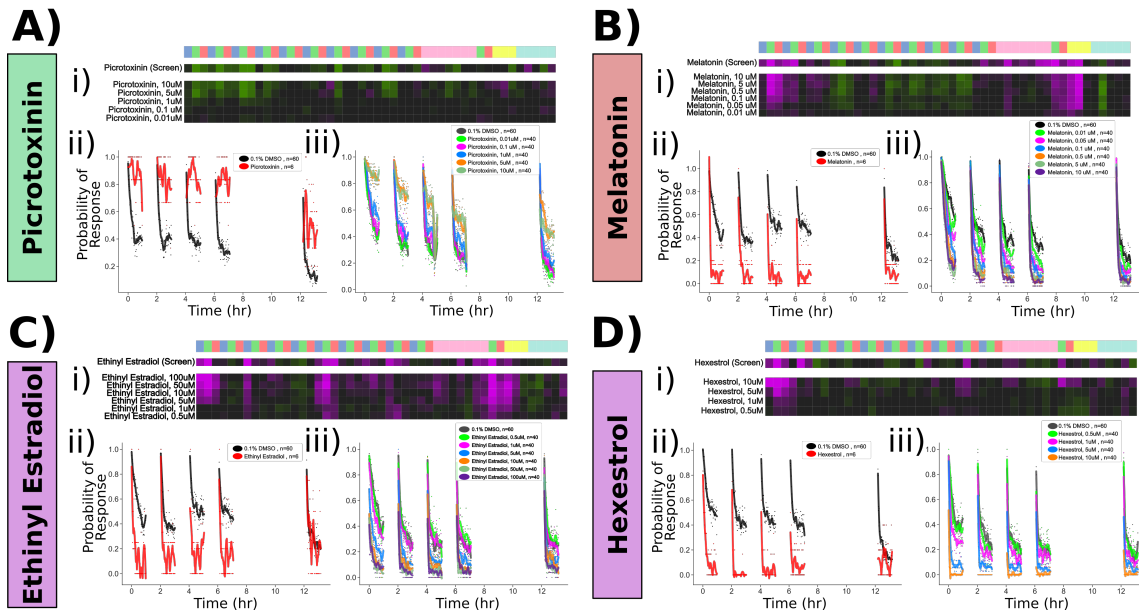


Figure 3. Confirmed pharmacological modulators of habituation.

Dose response studies for **A)** Picrotoxinin, **B)** Melatonin, **C)** Ethynodiol Estradiol and **D)** Hexestrol.

Displayed for each treatment are: i) Behavioural fingerprint for the original screen data (10 μ M), and the dose response data. ii) Original screen data for the probability of response to DF stimuli. Each dot is the probability of response to one flash. Lines are smoothed in time with a Savgolay Filter (window = 15 stimuli, order=2). iii) Dose response data for the probability of response, plotted as in ii)

Figure 3—figure supplement 1. Pharmacological manipulation of control behaviours and response displacement during habituation

and Picrotoxinin (PTX). PTX treatment had the strongest effects, with increased responsiveness to DFs during the training and test periods, indicative of defects in habituation (*Figure 2Ci*). Dose-response experiments confirmed a strong effect of PTX on inhibiting the progressive decrease in responsiveness during habituation learning at 1–10 μ M doses. Importantly, like the naive dark-flash response, the acoustic and optomotor response were not inhibited (*Figure 3A*, *Figure 3—figure Supplement 11A*). While strong GABA_{A/C}R inhibition will result in epileptic activity in larval zebrafish, we did not observe evidence of seizure-like behaviour at these doses, consistent with previous results *Bandara et al. (2020)*. Therefore, we conclude that partial antagonism of GABA_AR and/or GABA_CR is sufficient to strongly suppress habituation, indicating that GABA plays a very prominent role in habituation resulting in this strong sensitivity to manipulation. This is consistent with a model in which the potentiation of inhibition actively silences sensory-induced activity during habituation to suppress motor output, rather than the depression of excitatory neurotransmission in the activated pathway *Cooke and Ramaswami (2020); Ramaswami (2014)*.

We next turned our attention to the upper portion of the clustered behavioural fingerprint graph (*Figure 2A*), where strong and relatively specific inhibition of responsiveness during training and testing were observed, indicative of enhanced habituation (*Figure 2Cii, iii*). Among the hits observed here were multiple agonists of both Melatonin and Estrogen receptors, indicating that neuro-hormonal signaling may play a prominent role in plasticity underlying habituation. Dose response studies with Melatonin confirmed strong potentiation of habituation (*Figure 3B*). Melatonin did cause a decrease in spontaneous movement behaviour, consistent with its role in arousal/sleep regulation in zebrafish and other vertebrates *Gandhi et al. (2015); Zhdanova et al. (2001)*, yet Melatonin did not inhibit the naive response to dark flashes, the responsiveness to acoustic stimuli or OMR performance (*Figure 3B, Figure 3—figure Supplement 11A*), indicating it does not cause generalized sedation but modulates specific aspects of behaviour at these doses, including increasing habituation.

We similarly validated that the Estrogen Receptor agonists Ethynodiol Estradiol and Hexestrol, potentiated habituation at 5–100 μ M and 1–10 μ M doses, respectively (*Figure 3C,D*). However, Ethynodiol Estradiol strongly suppressed movement rates at these doses, and both treatments suppressed acoustic responsiveness and OMR performance

at doses $\geq 10\mu\text{M}$ (*figure Supplement 11C,D*). Therefore, it is less clear how specific or generalized Estrogen Receptor agonism is on behaviour, although the effective doses of Hexestrol for influencing habituation (1-5 μM) were lower than those that significantly affected other behaviours (10 μM). Nevertheless we decided to focus on PTX and Melatonin for the remaining experiments.

Our screening approach has identified both expected (GABA) and unexpected (Melatonin, Estrogen) pathways that strongly modulate habituation of responsiveness. We have also implicated multiple additional pathways in habituation, including Progesterone and PPAR α (*Figure 2C*), as well as OMR, acoustic and spontaneous behaviour, which can be mined for future projects investigating the molecular basis of behaviour.

Dark flash-induced neural activity is broadly inhibited during habituation

Having identified molecular components of habituation, we next aimed to identify how these molecules act within the circuit to modify neural activity and subsequent behavioural output. For this we used the MAP-Mapping strategy, which allows us to measure whole-brain activity patterns from freely-swimming larvae based on their relative levels of pERK immunostaining *Randlett et al. (2015)*. MAP-Mapping yields a picture of the activity patterns in the experimental setting that is closest to the drug-screen situation. We determined which areas of the brain respond to DFs by comparing the pERK patterns in larvae stimulated with 10 DFs at 1 min intervals, to those that were not stimulated (*Figure 4B, M*). These larvae were treated with 0.1% DMSO as a vehicle control for the pharmacological experiments (below). This revealed widespread activation of the brain in response to DFs, including visual areas such as the retina (ret), tectum (tec), pineal, pretectum and thalamus, indicating that a distributed sensory circuit is activated by DFs. However, relatively little signal was observed in the telencephalon or the habenula, indicating that these structures are not central to the DF response. Strong activation was seen in the hindbrain and cerebellum, likely reflecting motor-related signals related to the O-bend response.

We then asked how this pattern changes as the animals learn. We focused on a single training block of 60 DFs, as this is the period under which the strongest learning takes place, and where our chosen pharmacological treatments have the strongest effects relative to controls (*Figure 3*). Since the pERK indicator integrates over the last ≈ 15 minutes of life, but is biased towards the terminal 5 minutes *Randlett et al. (2015)*, these experiments were designed to highlight the final DFs after learning has taken place.

Indeed, these larvae showed much weaker activation across most of the brain (*Figure 4C, M*), which resulted in widespread decreases in neural activity compared to the 10 DF group (*Figure 4D, M*). This indicates that the plasticity underlying habituation affects neurons relatively early in the visual pathway, resulting in depressed activation in primary sensory areas (e.g. tectum and pretectum), as well as motor-related areas presumed to lie more downstream in the sensory-motor circuit (e.g. tegmentum and hindbrain). However, the retina was not depressed, indicating that habituation occurs downstream of this sensory structure.

To test our model of early visual pathway plasticity, we asked if the inhibition of habituation (via GABA_{A/C}R inhibition using PTX), or its potentiation (via Melatonin), led to the expected alterations in MAP-Maps. We first determined that Melatonin alone failed to strongly alter neural activity (*Figure 4E, M*), while PTX induced the expected activation associated with GABA inhibition, most prominently in the telencephalon (*Figure 4I,M*). Surprisingly, the naive response to DFs was potentiated in the Melatonin treatment and suppressed in the PTX treatment relative to their baseline activity, indicating that alterations in naive visual acuity for DFs is insufficient to explain the habituation phenotypes associated with these treatments (*Figure 4F,J,M*). Finally, when assaying for the depression of activity in trained fish relative to their naive response to DFs, we found that Melatonin treatment did indeed increase the observed depression, while PTX inhibited this depression, including in primary visual areas proximal to the retinal arborisation fields, the thalamus, pretectum, hypothalamus, and tectum neuropil (*Figure 4G,H,K-N*).

These whole-brain functional activity surveys demonstrate that habituation learning is associated with a surprisingly strong depression of neural activity, considering that at the behavioural level larvae remain quite responsive to DF stimuli after only one training block (Figure 1-3). These apparent discrepancies may reflect the presumably complex and non-linear relationship between neural activity and pERK responsiveness. Combined with the pharmacological manipulations, these experiments support a model in which habituation plasticity begins early in the visual pathway. However, the temporal and spatial resolution of these experiments is insufficient to differentiate how individual neurons adapt during habituation, and therefore do not exclude the possibility that habituation occurs within the retina, perhaps at the retinal ganglion cell terminals, where the central brain would simply receive

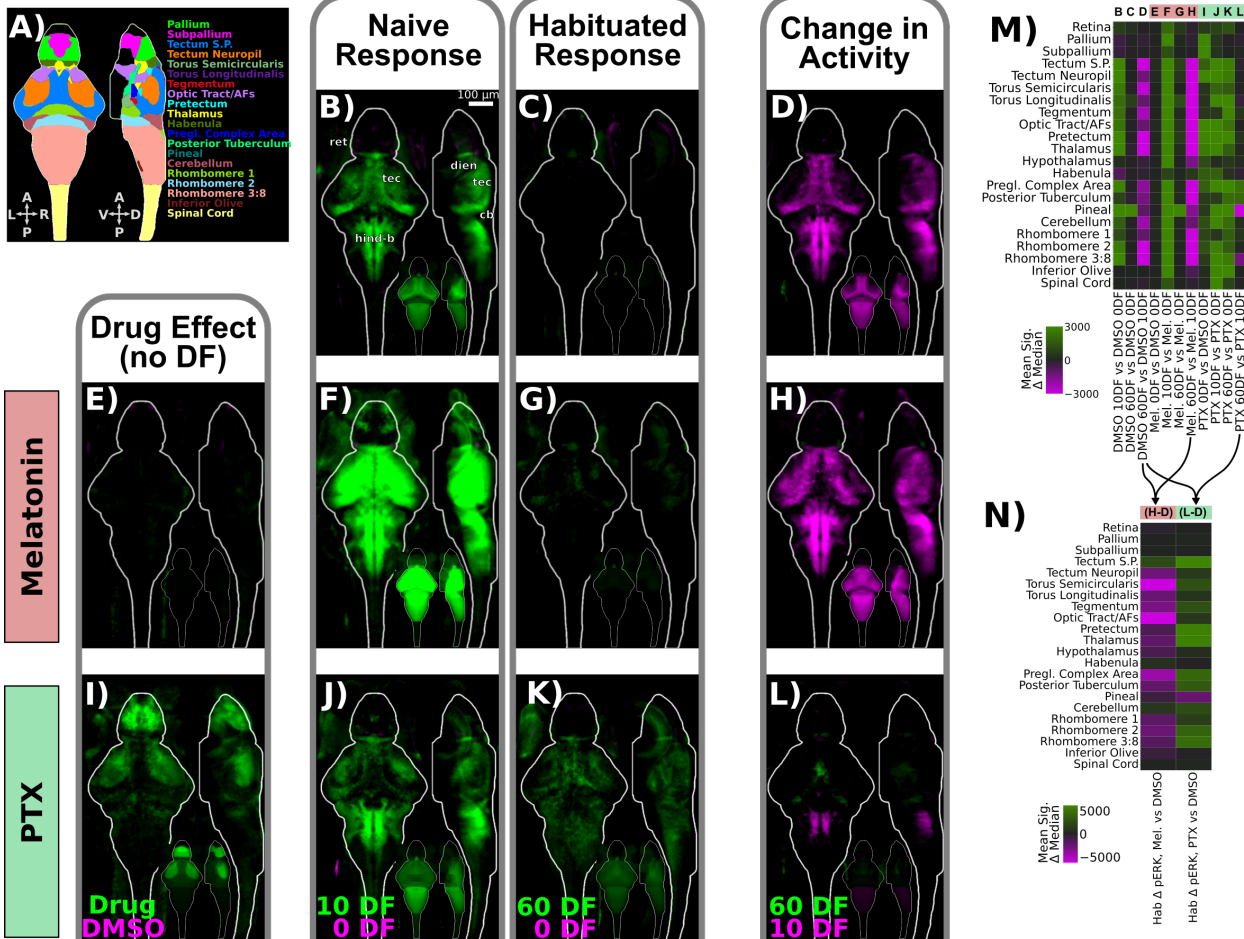


Figure 4. pERK-based whole-brain mapping of altered neural activity during habituation

A) Anatomical regions in the Z-Brain coordinate space used for image display and analyses. A = anterior, P = posterior, L = left, R = right, V = ventral, D = dorsal.

B-L) MAP-Maps showing areas with whole-brain differences in pERK/tERK staining intensity, with green and magenta representing significantly increased staining in the relevant group in the pairwise comparison. Shown as summed intensity projections in the Z-Brain coordinate space in the dorso-ventral (left) and sagittal (right) dimensions. Lower inset represents the average signal binned by brain regions. MAP-Maps were calculated for pairwise differences between the following treatments in: Column 1: "Drug Effect (no DF)" = drug treatment with no stimulation (green) vs. DMSO with no DFs (magenta) Column 2: "Naive Response" = Response to 10 DFs (green) vs. 0 DFs (magenta) Column 3: "Habituated Response" = Response to 60 DFs (green) vs. 0 DFs (magenta) Column 4: "Change in Activity" = Response to 60 DFs (green) vs. 10 DFs (magenta). Pharmacological treatments arranged in rows as: Row 1 0.1% DMSO Row 2 Melatonin, 0.1 μ M in 0.1ret Row 3 Picrotoxinin (PTX), 5 μ M in 0.1ret = retina, dien = diencephalon, tec = tectum, cb = cerebellum, hind-b = hindbrain

M) Mean signal in brain regions for each of the experiments shown in A-K, shown as a vector in the heatmap. Same data as insets in A-K

N) Difference in the MAP-Map signals in brain areas comparing drug treated fish to DMSO control when stimulated with 60 DF vs 10 DF. Resultant differences reflect altered activity during habituation training by the drug treatment. Number of imaged fish per experimental group were: 0.1% DMSO, 0 DF = 26; 0.1% DMSO, 10 DF = 29; 0.1% DMSO, 60 DF = 23; Melatonin, 0 DF = 29; Melatonin, 10 DF = 23; Melatonin, 60 DF = 19; Picrotoxinin, 0 DF = 28; Picrotoxinin, 10 DF = 23; Picrotoxinin, 60 DF = 27. DF = Dark Flash, Mel = Melatonin, PTX = Picrotoxinin.

an increasingly depressed signal from the periphery.

Volumetric 2-photon Ca^{2+} imaging of habituation learning

Having identified the regional alterations in activity associated with habituation learning, we next asked how the properties of individual neurons within the DF responsive circuit adapt during habituation. We used a head-fixed paradigm to perform 2-photon Ca^{2+} imaging during habituation learning. We expressed nuclear-targeted GCaMP7f pan-neuronally and imaged with a resonant scanner and piezo objective, enabling us to cover a volume of $\approx 600 \times 300 \times 120 \mu\text{m}$ (x,y,z) sampled at $0.6 \times 0.6 \times 10 \mu\text{m}$ resolution, leading to the detection of 30890 ± 3235 ROIs per larvae ($\pm \text{SD}$, *Figure 5A,C*). ROIs were aligned to the Z-Brain atlas coordinates *Randlett et al. (2015)*, demonstrating that this volume spans most of the areas implicated in DF habituation by our MAP-Mapping experiments (*Figure 4*), including the majority of the midbrain, hindbrain, pretectum and thalamus (*Figure 5A-C*). Visual stimuli were delivered via a red LED, and larvae were stimulated with 60 DFs at 1 min intervals to induce habituation learning. This induced strong Ca^{2+} activity in neurons (*Figure 5C*), some of which were clearly associated with the DF stimuli. Ca^{2+} transients in response to DFs generally decreased across the 60 stimuli, though this pattern was not seen in all neurons, and substantial heterogeneity in their adaptations were observed. Strong correlated patterns were also seen in large groupings of neurons, predominantly in the hindbrain, which were associated with movement events through their correlation with motion artifacts in the imaging data (*Figure 5-figure Supplement 1*).

To explore the spatial patterns in these datasets we used a 2-dimensional lookup table to simultaneously visualize the correlation and bias of Ca^{2+} fluctuations with regressors representing either DF stimuli or movement (*Figure 5E, F*). This revealed segregated populations of neurons coding for the DFs (pink) and movement (green/teal). Similar patterns are visible in individuals and across the entire population of 34 larvae. As expected, DF-tuned neurons were located predominantly in visual sensory areas in the midbrain (tectum) and diencephalon (pretectum and thalamus). Motor-coding neurons dominated in the hindbrain, with the exception of the cerebellum and inferior olive, which was predominantly tuned to the sensory stimulus. Some neurons did show approximately equal correlation values to both stimuli, as evidenced by the blue-ish hues. Finally, some areas of the brain appeared to contain mixtures of neurons with different coding properties, including the ventral diencephalon and midbrain.

To determine if there was any spatial logic to how different neurons adapt their responsiveness to DFs during imaging we plotted the ROIs using a lookup table highlighting the preference of ROIs for either the first three DFs (pink, naive response), or last three DFs (green, trained response). Strong preferences for the naive stimulus reflects a depressing response profile (*Figure 5G, H*). Indeed, most neurons did show tunings consistent with strong depression, however there were neurons who showed an equal preference for naive and trained stimuli, or even stronger preference for the latter, indicating stable or potentiating response profiles. These non-depressing neurons were mostly contained in the dorsal regions of the brain, including the torus longitudinalis, cerebellum and dorsal hindbrain. These results demonstrate that while the majority of neurons across the brain depress their responsiveness during habituation, a smaller population of neurons exists that show the opposite pattern.

From these experiments we conclude that habituation does not occur exclusively within the retina, as in such a model neurons that show stable responses or that potentiate would not be present in the brain. Instead, these data are consistent with the model arising from our pERK analysis, where habituation begins early within the visual pathway, but downstream of the retina. However, the fact that non-depressing neurons are observed within structures like the caudal hindbrain and the cerebellum demonstrates that motor-related brain regions contain non-depressed signals, and thus plasticity could also be occurring in regions very downstream in the visual sensory-motor pathway.

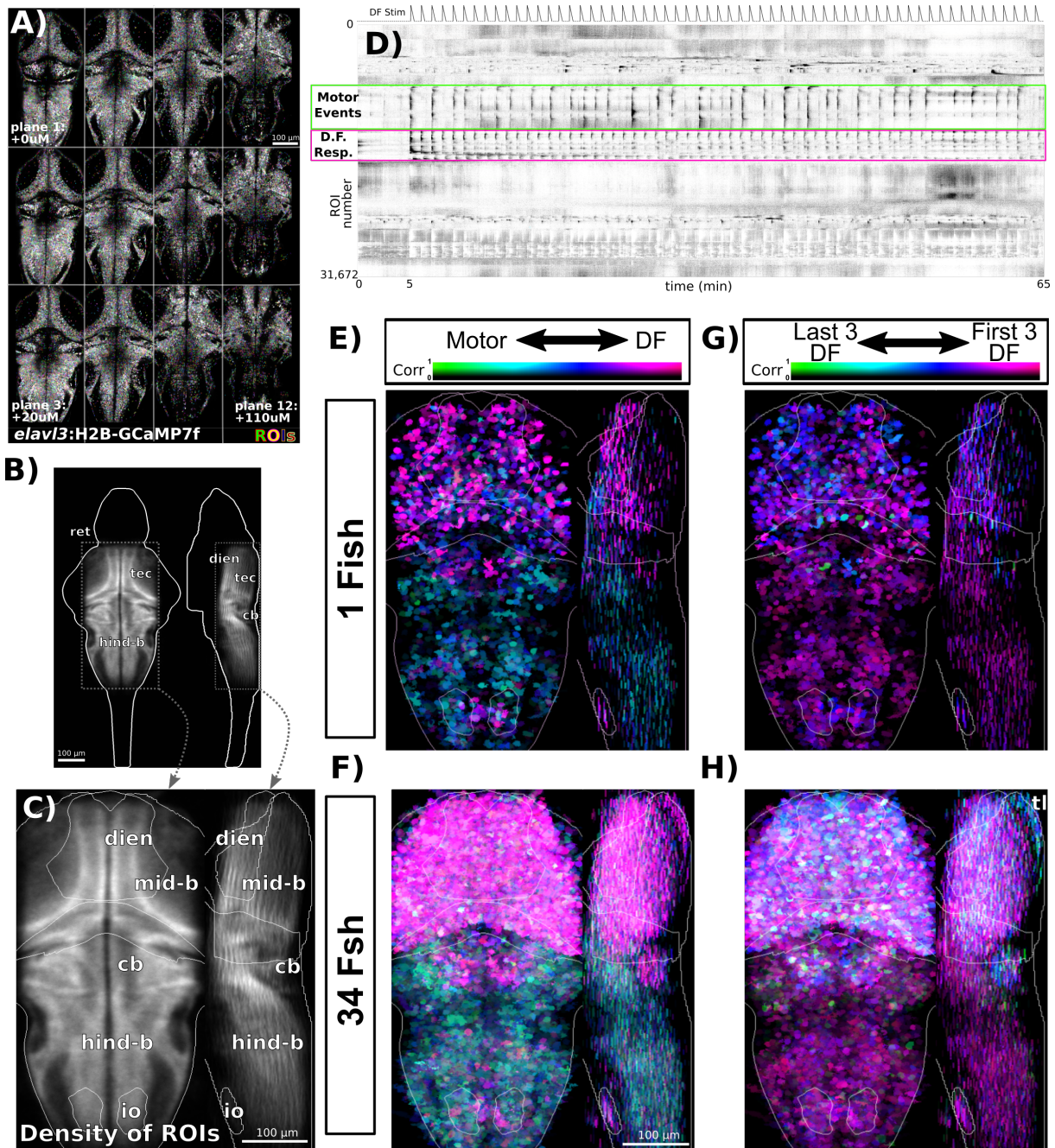


Figure 5. Volumetric 2-photon Ca^{2+} imaging of dark flash habituation.

A) *Tg(elavl3:H2B-GCaMP7f)* larvae were imaged across 12 z-planes at $10\mu\text{m}$ steps. ROIs segmented using suite2p **Pachitariu et al. (2017)** are overlaid in random colors.

B) Density of detected ROIs registered and plotted in the Z-Brain coordinate space. $n=1,050,273$ ROIs across 34 larvae.

C) Cropped field of view used for plotting and analyzing Ca^{2+} imaging data and approximate anatomical localizations of major brain areas: dien=diencephalon, mid-b = midbrain, cb = cerebellum, hind-b = hindbrain, io = inferior olive, ret = retina, tec = tectum

D) Functional responses of the population of neurons in the same fish as A), plotted as a clustered heatmap ("rastermap" **Pachitariu et al. (2017)**, github.com/MouseLand/rastermap), where rows represent individual neurons ordered by the similarities in their activity. Darker shades reflect increased activity. This clustering reveals neurons that are tuned to the DF stimuli (pink box) or motor events (green box). Dashed trace above the heatmap depicts the DF stimulus convolved with a kernel approximating H2B-GCaMP7f kinetics.

E) ROIs in an individual fish plotted based on their correlation and tuning to regressors defining either Motor or DF stimulus events, highlighting the spatial distributions of these tunings across the imaged population. Plotted as a maximum intensity projection.

F) Same analysis as E, but across the entire population of 34 larvae.

G) ROIs in an individual fish plotted based on their correlation and tuning to regressors defining either the first or last three DF stimuli.

H) Same analysis as G, but across the entire population of 34 larvae. tl = torus longitudinalis

Figure 5—figure supplement 1. Validation of motion analysis based on image artifacts during 2-photon imaging

Functional classification and anatomical localization of neuronal types observed during habituation learning

To categorize the functional heterogeneity within the DF-tuned neurons we used affinity propagation clustering. This method has the advantage that cluster number does not need to be defined beforehand, and attempts to identify the most representative response profiles algorithmically *Förster et al. (2020)*. This identified 12 clusters that differed both in their adaptation to repeated DFs, as well as the shape of their response to the DF (*Figure 6A,B*).

We therefore use these two dimensions of the response to label the clusters:

Adaptation Profile: (Depression vs. Potentiation)

No Adaptation = noA : Cluster 1, 9, 10

Weak Depression = weakD : Cluster 5, 6, 11

Medium Depression = medD : Cluster 2, 3, 7

Strong Depression = strgD : Cluster 4, 8

Potentiation = Pot : Cluster 12

Response Shape: (Transient/Short vs. Sustained/Long)

On-response = $_{On}$: Cluster 1, 2

Long/sustained response = $_L$: Cluster 3, 4

Medium-length response = $_M$: Cluster 5, 6, 9

Short/transient response = $_S$: Cluster 7, 8, 10, 11

Yielding clusters: $1_{On}^{noA}, 2_{On}^{medD}, 3_L^{medD}, 4_L^{strgD}, 5_M^{weakD}, 6_M^{weakD}, 7_S^{medD}, 8_S^{strgD}, 9_M^{noA}, 10_S^{noA}, 11_S^{weakD}$, and 12_M^{Pot}

While these results indicate the presence of a dozen functionally distinct neuron types, such cluster-based analyses will force categories upon the data irrespective of if such categories actually exist. To determine if our cluster analyses identified genuine neuron types, we analyzed their anatomical localization (*Figure 6C, D*). Since our clustering was based purely on functional responses, we reasoned that anatomical segregation of these clusters would be consistent with the presence of truly distinct types of neurons. Indeed, we observed considerable heterogeneity both within and across brain regions. For example: 11_S^{weakD} was mostly restricted to medial positions within the optic tectum; 3_L^{medD} and 4_L^{strgD} were more prevalent within motor-related regions of the brain including the Tegmentum and Hindbrain Rhombomeres; 9_M^{noA} was the most prominent cluster in the torus longitudinalis, consistent with the presence of non-depressing signals in the area (*Figure 5G,H*).

We then quantified the similarity in the spatial relationships among the clusters by looking at the correlations in the positions of the ROIs in downsampled super-voxels of the Z-Brain (*Figure 6E*). This revealed similar hierarchical relationships to those identified functionally (*Figure 6B*), especially with respect to *Response Shape*, indicating that physical proximity is predictive of the functional similarity of neurons, even across clusters.

Finally, since our functional analysis was performed purely based on correlations with the DF stimuli, we asked to what extent neurons belonging to each cluster were correlated with motor output. This identified 4_L^{strgD} as the most strongly correlated to motor output, consistent with its strong habituation profile and its localization within motor-regions of the hindbrain. This indicates that 4_L^{strgD} neurons likely occupy the most downstream positions within the sensory-motor network.

These results highlight a diversity of functional neuronal classes observed during DF habituation. Whether there are indeed 12 classes of neurons, or if this is an over- or under-estimate, awaits a full molecular characterization. However, we proceed under the hypothesis that these clusters define neurons that play distinct roles in the DF response and/or its modulation during habituation learning.

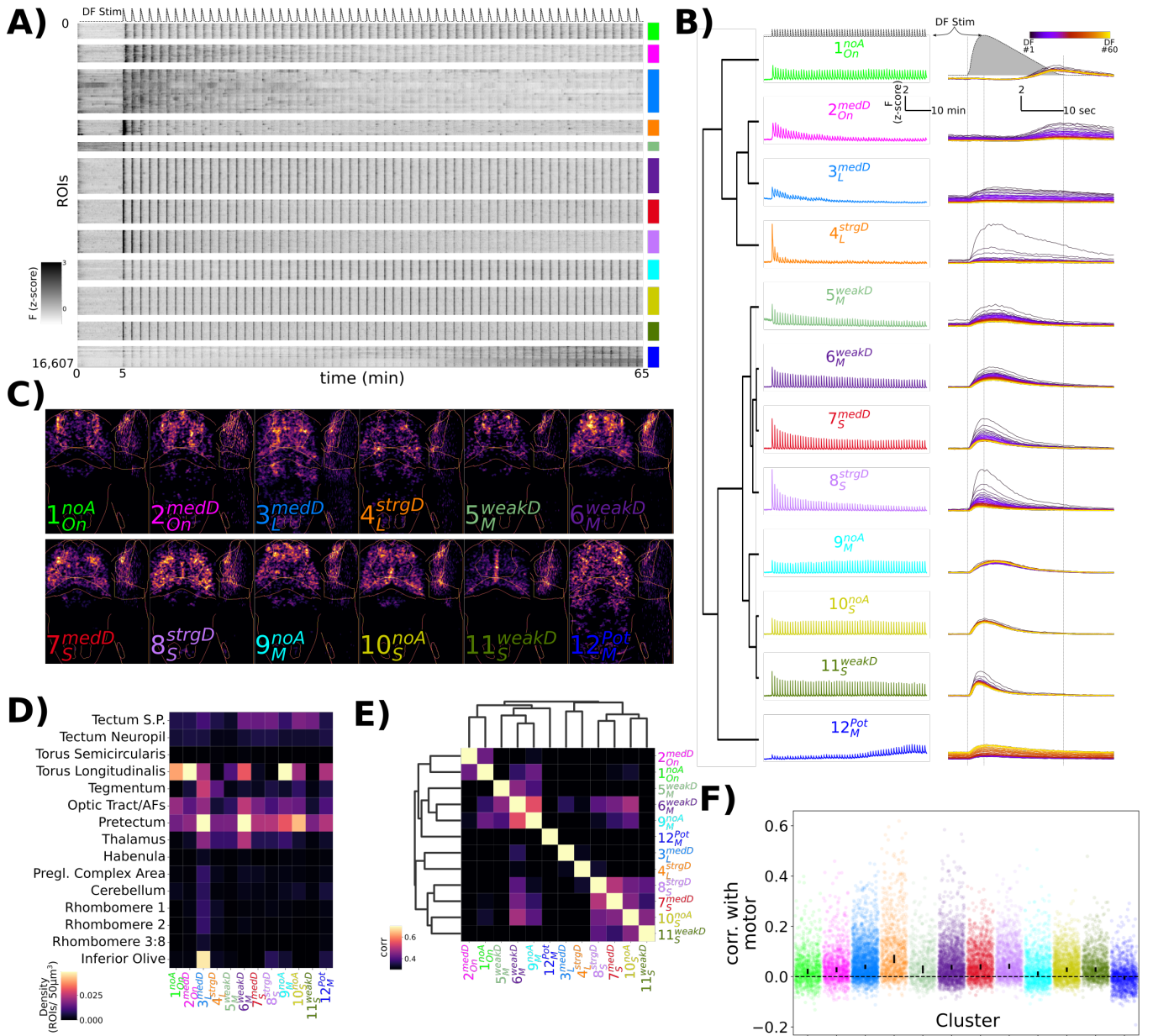


Figure 6. Characterization of functional response types during habituation learning.

- A)** Heatmap of the response profiles of ROIs categorized into 12 functional clusters. n=16,607 ROIs from 34 larvae.
- B)** Average z-scored fluorescence of each functional cluster plotted for the whole experiment (left column), and centered on each DF stimulus (right column), demonstrating the differences in both *Adaptation Profiles* and *Response Shape* for each cluster. Clusters were identified using Affinity Propagation clustering (affinity = Pearson correlation, damping = 0.9, preference = -9), and organized using Hierarchical clustering, distance = complete, correlation. Dashed lines in top panels are the DF stimulus convolved with a kernel approximating H2B-GCaMP7f kinetics, used as the regressor in the analysis.
- C)** Summed intensity projection of the ROIs belonging to each functional cluster in Z-Brain coordinate space depicting their physical locations in the brain. Projection images are normalized to the maximum value.
- D)** Heatmap depicting the density of each cluster that is found within different Z-Brain regions.
- E)** Correlogram calculated from the Pearson correlation in downsampled volumes for the ROI centroid positions for each cluster (see Methods). Hierarchical clustering, distance = complete, correlation.
- F)** Correlation between motor events and the Ca²⁺ traces for each ROI assigned to the functional clusters. dots = individual ROIs, bar height = 99.9999% confidence interval around the median value.

Identification of GABAergic inhibitory neurons during habituation

How might the functional classes of neurons we identified interact within a circuit to drive habituation behaviour? Considering that we have implicated GABAergic inhibition in habituation, the simplest model would assign a GABAergic identity to the potentiating neurons; 12_M^{Pot} . These inhibitory neurons would then act to progressively increase inhibition during learning (*Figure 7A*, Model 1). Potentiation of these neurons could be achieved through, for example, LTP at their inputs during learning.

A limitation of the pan-neuronally expressed GCaMP imaging approach is the lack of knowledge as to the molecular identity of neurons, such as neurotransmitter type. Virtual co-localization analyses with 3D atlases can be used to identify candidate molecular markers for functionally identified neurons, provided sufficient stereotypy exists in neuronal positioning, and the relevant marker exists in the atlas *Dunn et al. (2016)*; *Randlett et al. (2015)*. Therefore, we analyzed the spatial correlations for markers contained in the Z-Brain *Randlett et al. (2015)*, Zebrafish Brain Browser *Gupta et al. (2018)*; *Marquart et al. (2017)*; *Tabor et al. (2018)*, and mapZebrain atlases *Kunst et al. (2018)*; *Shainer et al. (2022)*. We identified markers showing the highest spatial correlations with any of our functional clusters (corr. > 0.15, n=89 of 752 markers), and organized these hierarchically (*Figure 7B*).

We were particularly interested in associations with GABAergic neurons labeled by the *gad1b* reporter lines. These were located in a region of the hierarchy showing greatest spatial similarity with 10_S^{noA} and 11_S^{weakD} (*Figure 7C*). An enrichment along the medial tectum is common to markers in this region of the hierarchy, where the highest density of GABAergic neurons within the tectum reside. Contrary to Model 1, 12_M^{Pot} neurons did not appear to be associated with GABAergic neuronal markers in this analysis.

These data indicated that 10_S^{noA} and 11_S^{weakD} neurons are the predominant GABAergic classes. To test this, we imaged the response of neurons in *Tg(Gad1b:DsRed);Tg(elavl3:H2B-GCaMP6s)* double transgenic larvae, and classified neurons as *gad1b*-positive or -negative based on DsRed/GCaMP levels (*Figure 7D*). Indeed we saw a heterogeneous distribution of *gad1b*-positive neurons across functional clusters, including a significant enrichment in not only 10_S^{noA} and 11_S^{weakD} , but also the other two clusters with the "Short" Response Shape (7_S^{medD} and 8_S^{strgD} , *Figure 7E*). The remaining clusters either showed no significant bias, indicating that they contain mixed populations, or a significant depletion of *gad1b*-positive cells, suggesting that they comprise mostly of excitatory or neuromodulatory neurons (3_L^{medD} and 12_M^{Pot}).

Therefore, these results are inconsistent with Model 1, since 12_M^{Pot} neurons appear to be mainly non-GABAergic. Instead, GABAergic neurons span the remainder of the range of adaptation profiles, from non-adapting to strong-depressing. These neurons are best characterized by the shape of their response to the stimulus, perhaps reflecting a transient bursting style of activity relative to other neuronal types that exhibit more sustained firing patterns.

A pharmacologically-constrained model of the habituating circuit

Our functional and anatomical analyses indicate that distinct populations of GABAergic neurons exist that inhibit behavioural responsiveness during learning. What connectivity and plasticity mechanisms might underlie the relationships between these neurons, and how do they shape the functional patterns of other neurons in the circuit? We currently do not have sufficient anatomical knowledge to realistically constrain such models. However, if we approach this problem with Occam's razor with respect to the mechanism of plasticity we arrive at a model in which the global potentiation of GABAergic synapses drives habituation. Potentiation of GABAergic output through inhibitory long-term potentiation (i-LTP) could explain why GABAergic neurons do not potentiate in their firing pattern, but still exhibit increasing influence over the circuit during habituation. Assuming that excitatory activation in the circuit is consistent, differential connectivity weights between GABAergic neurons and the other neuronal classes could drive the differential rates of depression: i-LTP at strong GABAergic connections drives strong depression, while i-LTP at weak GABAergic connections drives weak depression (*Figure 8A*, Model 2).

To test this model, we asked how PTX and Melatonin influence the dynamic activity states in different classes of neurons. Antagonism of GABA receptors via PTX should decrease the influence of these inhibitory neurons on the remaining populations, shifting the balance from strong depression towards weaker or non-adapting response profiles. We have found that Melatonin potently increases habituation behaviour (*Figure 3*), and further depresses brain-wide neuronal activity during habituation beyond normal levels (*Figure 4*). These are effectively opposite of the effect of PTX, and thus we hypothesized that Melatonin acts in concert with GABA in the circuit, shifting the balance towards strongly depressing profiles. This model of the action of Melatonin also fits with the observations that

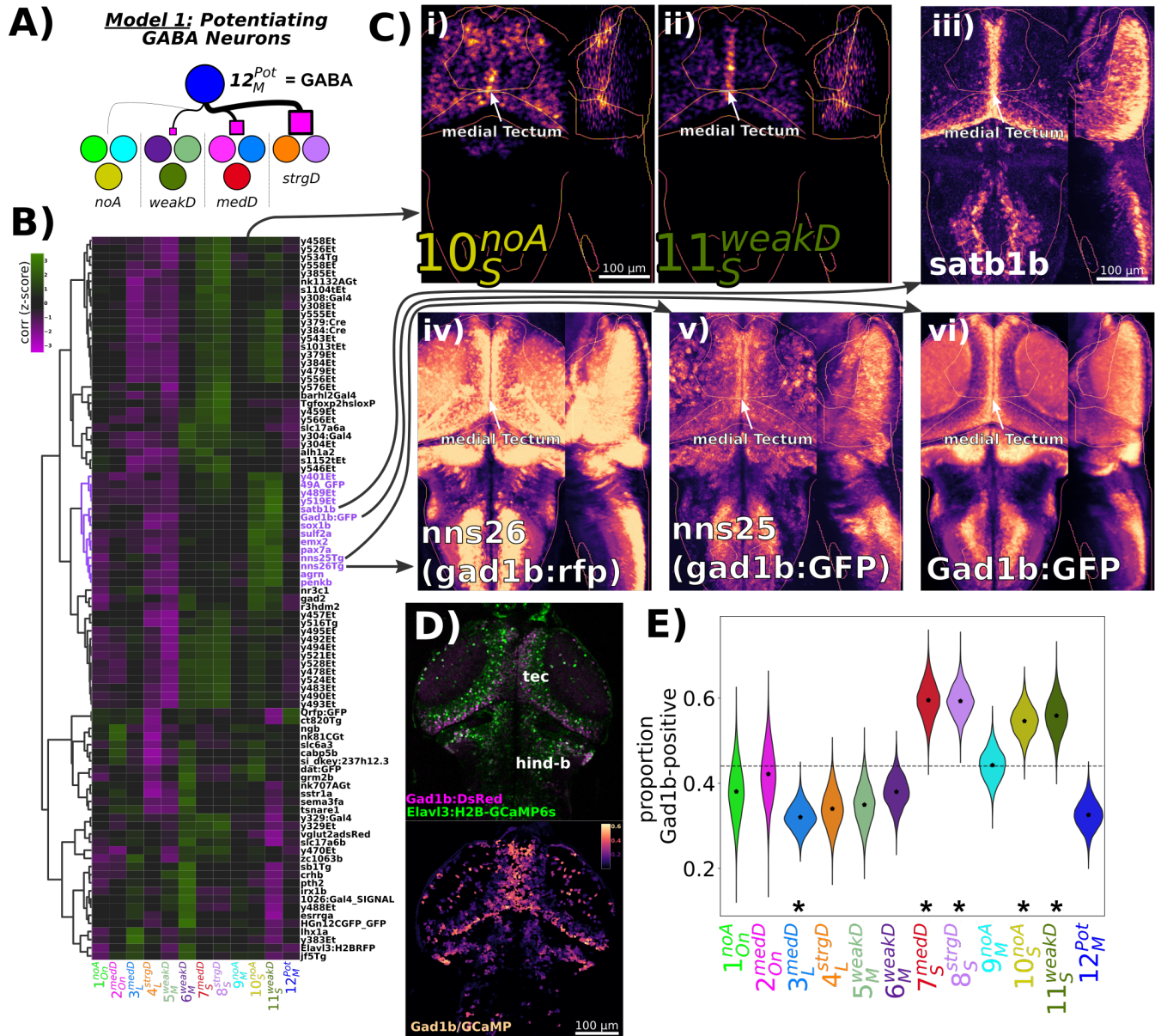


Figure 7. An atlas-based search for molecular markers identifies GABAergic neuronal classes.

A) Model 1, proposed to explain how potentiating GABAergic inhibition could mediate the range of depressive adaptations observed during habituation. Model posits that the sensitizing neurons are GABAergic (12_{M}^{Pot} , blue), and they differentially connect to functional subtypes: Strong connectivity to strongly habituating classes, weak connectivity to weakly habituating classes, etc.

B) Hierarchically clustered heatmap depicting the correlation of markers aligned to the Z-Brain atlas with the spatial arrangement of the 12 functional clusters (distance = complete, correlation). Correlation values are z-scored by rows to highlight the cluster(s) most strongly correlated or anti-correlated with a given marker. The subset of the hierarchy containing the *gad1b*-reporters is coloured in purple.

C) Normalized summed intensity projections comparing the spatial arrangements of i) 10_{S}^{noA} , and ii) 11_{S}^{weakD} with atlas markers found within the purple cluster iii) *satb1b* HCR (Shainer et al., 2022), mapZebrain Atlas iv) *nns25*, aka *TgBAC(gad1b:GFP)* (Satou et al., 2013), mapZebrain Atlas v) *nns26*, aka *TgBAC(gad1b:LOXP-RFP-LOXP-GFP)* (Satou et al., 2013), mapZebrain Atlas vi) *TgBAC(gad1b:GFP)* (Satou et al., 2013), Z-Brain Atlas

D) 2-photon imaging of *Tg(Gad1b:DsRed);Tg(elavl3:H2B-GCaMP6s)* larvae depicting the raw data for each channel (top), and the ratio of Gad1b/GCaMP6s fluorescence in each ROI functionally identified using suite2p.

E) ROIs imaged in double transgenic larvae are assigned a cluster identity based on their correlation to the cluster mean trace, and classified as Gad1b-positive based on a DsRed/GCaMP6s ratio of greater than 0.25. Dotted line = expected proportion based on total number of cells classified as Gad1b-positive. * $p < 0.05$, Chi Square test with Bonferroni correction. Distributions underlying violin plots calculated by bootstrapping 5000 replicates. $n = 1835$ ROIs in 6 larvae.

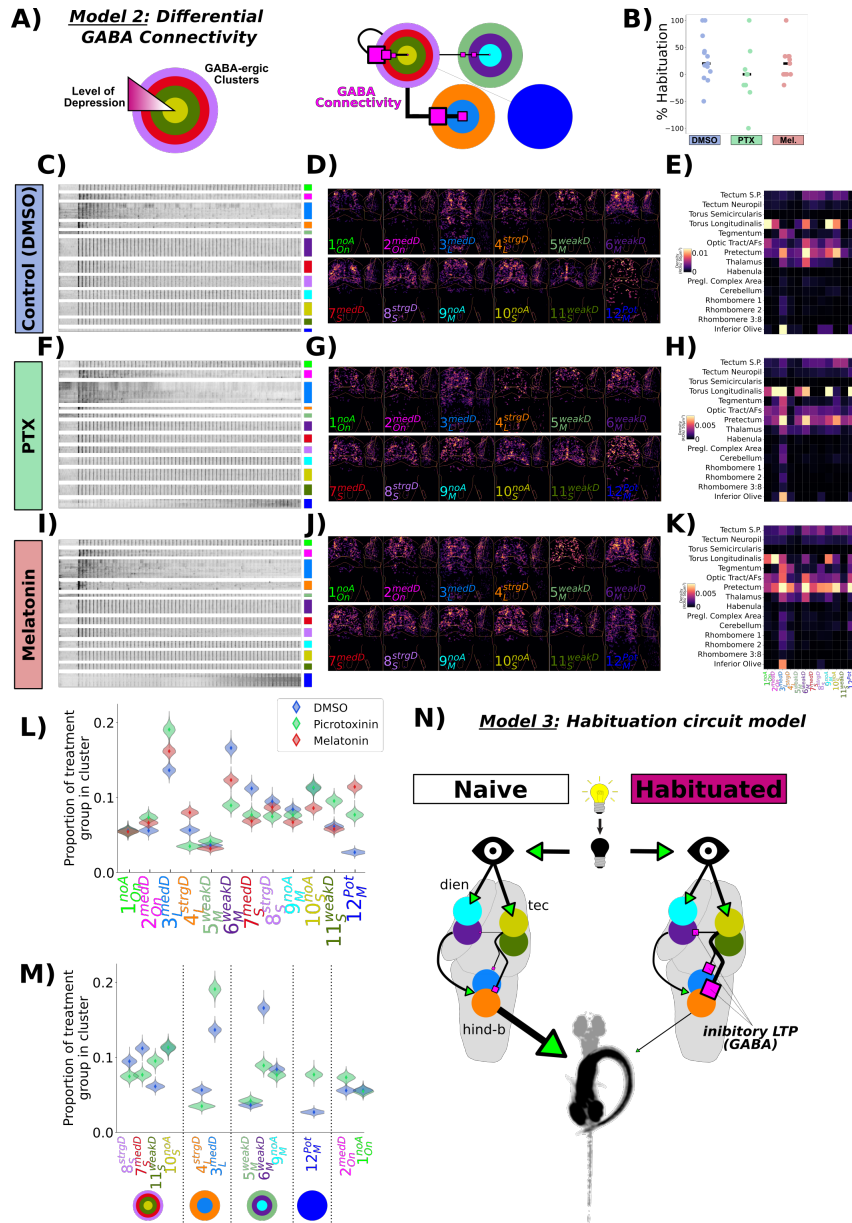


Figure 8. A pharmacologically constrained model for dark flash habituation

A) *Model 2*, proposed to explain how biased GABAergic inhibition could mediate the differential habituation rates observed across functional classes of neurons. Model proposes that the neurons with the Short Response Shape are GABAergic, and that they differentially connect to the other functional subtypes, as well as themselves to drive the response decreases observed during habituation. The strength of this inhibitory connectivity determines the decrease in responsiveness across neuronal classes. Larger pink box = Stronger inhibition.

$$\text{Percent Habituation} = 100 \times (1 - \frac{P(\text{Resp}_{31-60})}{0.5 \times (P(\text{Resp}_{1-30}) + P(\text{Resp}_{31-60}))})$$

C-K) Functional clustering of neurons from larvae treated with DMSO (vehicle control), Picrotoxinin (PTX, 10 μ M), or Melatonin (1 μ M). C,F,I) Heatmap of response profiles of ROIs categorized into the 12 functional clusters. D,G,J) Summed intensity projection of the ROIs belonging to each functional cluster in Z-Brain coordinate space depicting their physical locations in the brain. Projection images are normalized to the maximum value. E,H,K) Heatmap depicting the density of each cluster that is found within different Z-Brain regions. C-E) DMSO, n = 428,720 total ROIs in 14 larvae F-H) Picrotoxinin (PTX), n = 271,037 total ROIs in 9 larvae I-K) Melatonin treatment, n = 350,516 total ROIs in 11 larvae. **L)** Proportion of neurons belonging to each functional cluster across treatment groups. Distributions for violin plots are bootstrapped from 5000 replicates.

M) Same data as M, only showing the data for PTX vs DMSO vehicle control, re-ordered to reflect the cluster Adaptation Profiles.

N) *Model 3*, proposed circuit model for the habituation of the probability of responding to a DF stimulus. The dark flash stimulus is detected by the retina and sent as an unadapted signal to the brain. GABA-ergic inhibitory neurons form the critical node in the habituating circuit, where habituation occurs as the result of a potentiation of GABAergic synapses, resulting in depressed responses in connected neurons. The strength of neuronal adaptation during habituation depends on the GABAergic connectivity strength (as in *Model 2* (A)). The output neurons of the circuit are the Long-responding class. Potentiated GABAergic inhibition onto this population silences behavioural output.

Figure 8—figure supplement 1. Mean response of functionally identified clusters after different pharmacological treatments

Melatonin can directly potentiate the effects of GABA [Cheng et al. \(2012\)](#); [Niles et al. \(1987\)](#). Alternatively Melatonin may signal through one of 6 known G-protein coupled receptors in larval zebrafish [Maugars et al. \(2020\)](#), which could act to modulate activity states in GABAergic neurons or their targets.

We compared the Ca²⁺ activity patterns in neurons from fish treated with vehicle (0.1% DMSO), PTX, or Melatonin ([Figure 8B-M](#)). At the behavioural level, we found a trend indicating that we were able manipulate habituation pharmacologically in our tethered imaging assay, though this was very subtle ([Figure 8B](#)). This discrepancy relative to the very strong behavioural effects in freely-swimming animals ([Figure 3](#)) likely result from the head-restrained protocol, which itself strongly inhibits behavioural output. Therefore assaying for habituation at the behavioural level is difficult to interpret. Alternatively, drug access to the brain may have been compromised by the agarose mounting resulting in weaker behavioural effects. Yet, since we did observe a trend in behavioural data, we proceeded under the assumption that the drugs were having the desired effects.

We examined the activity profiles of neurons that belonged to the 12 different functional clusters. Surprisingly, we observed no strong alterations of the response profiles of these neurons ([Figure 8C-K](#), [Figure 8-figure Supplement 1](#)). However, what was clearly altered was the proportion of neurons that belonged to different functional classes ([Figure 8L,M](#)).

From these analyses we conclude the following:

- A)** The pharmacological manipulations did not alter the activity of neurons in such a way as to alter the average activity states of the population within each cluster ([Figure 8-figure Supplement 1](#)). Instead, the proportion of neurons belonging to different functional classes changed. This may result from our classification scheme, or could point to fixed and relatively inflexible processing strategies that the brain is using in the context of dark-flash habituation.
- B)** The effect of PTX on cluster reassignment generally followed the type of effects predicted from [Model 2](#), increasing the proportion of cells falling into the weaker depressing classes ([Figure 8M](#)). This pattern was most clear in the classes with "Short" and "Long" *Response Shapes*, which are those that included the most strongly depressed classes of neurons, and would thus be the most influenced by GABA-mediated inhibition. Non-depressing classes were not strongly modulated, consistent with a model that these neurons receive little GABAergic input. Therefore, we conclude that [Model 2](#) is consistent with much, but not all of the alterations in response to PTX. For example, PTX increased the proportion of 6_M^{weakD} neurons, which does not follow from [Model 2](#).
- C)** Based on our hypothesis that the effect of Melatonin is to potentiate GABAergic inhibition, we expected PTX and Melatonin to have opposite effects. Similar to (B), this hypothesis is not fully supported by all of the data, but is consistent with the observations in a subset of functional classes, perhaps those that are most critical for the habituation of response probability. Indeed, the expected opposite effects of PTX and Melatonin were present in two of the most conspicuous functional classes: 4_L^{strgD} , which is most strongly correlated with motor output and thus is most closely associated with behavioural initiation ([Figure 6F](#)), and 11_S^{weakD} , which showed the clearest GABA-like anatomical pattern in the tectum.
- D)** One of the most interesting classes of neurons we observed during habituation are those that potentiate their responses (12_M^{pot}). Remarkably, both Melatonin and PTX increased the proportion of neurons within this class. This result, combined with our observation that these cells are non-GABAergic ([Figure 7E](#)), strongly suggests that the role of these cells is not simply to suppress activity in the circuit to inhibit behavioural responses (as in [Model 1](#)). The functional role played by this class of neurons during habituation remains mysterious. However, it may relate to some of the common behavioural effects of Melatonin and PTX, such as the inhibition of habituation when measuring response Displacement ([Figure 3A,B](#), [Figure 3-figure Supplement 1E, F](#)).

Based on these data we propose a working model of the dark flash habituation circuit, particularly focused on the elements we have implicated in the decreasing probability of response ([Figure 8N](#), [Model 3](#)). At the center are the GABAergic synapses, whose progressive potentiation drives habituation. Their influence on the depression of excitatory neurons in the circuit is biased based on their connectivity weights, where strong connectivity drives strong-habituation. Silencing of the long-responding motor-related neurons (4_L^{strgD}) suppresses O-bend responses. PTX acts upon the outputs of the GABAergic neurons to decrease their influence in the circuit, thus inhibiting habituation. Melatonin acts either by directly potentiating the action of GABA at the synapse (Cheng et al., 2012; Niles et

al., 1987), or by decreasing the excitability of postsynaptic neurons.

Discussion

Molecular mechanisms of DF habituation

In the pharmaco-behavioural data resulting from our screen, we focused our analysis on those pharmacological agents and pathways that strongly and relatively specifically modulated habituation when measuring response probability. We found that inhibition of GABA_{A/C} Receptors using PTX reduced habituation learning. GABA is the main inhibitory neurotransmitter in the zebrafish brain, and deficits in GABA signaling lead to epileptic phenotypes *Baraban et al. (2005)*. We were fortunate that our screening concentration (10μM) did not induce seizures, but was still sufficient to inhibit habituation. This implies that the habituation circuit is exquisitely sensitive to changes in GABA signaling at levels well below the threshold required to globally change excitatory-inhibitory balances. This argues for a central rather than supporting role of GABAergic inhibition in dark-flash habituation.

A critical role for GABA in habituation is consistent with data from *Drosophila*, where both olfactory and gustatory habituation have been linked to GABAergic interneurons *Das et al. (2011); Paranjpe et al. (2012); Trisal et al. (2022)*. Therefore, this circuit motif of increasing inhibition to drive habituation may be a conserved feature of habituation, which would allow for a straightforward mechanism for habituation override during dis-habituation via dis-inhibition *Cooke and Ramaswami (2020); Trisal et al. (2022)*.

Our screen also identified that neuro-hormonal signaling is critical for habituation, where Melatonin and Estrogen receptor agonists potently increase habituation learning rate. The role of Estrogens in learning and memory is well established *Luine et al. (1998); Nilsson and Gustafsson (2002)*. Though its role in habituation is less well explored, it has previously been shown to increase memory retention for olfactory habituation in mice *Dillon et al. (2013)*. To our knowledge, Melatonin has not previously been implicated in habituation, though it has been implicated in other learning paradigms *El-Sherif et al. (2003); Jilg et al. (2019)*. Notably, Melatonin was shown to block operant learning at night in adult zebrafish *Rawashdeh et al. (2007)*, and therefore Melatonin appears to be able to both promote or inhibit plasticity in zebrafish, depending on the paradigm.

While Melatonin and Estrogen were not strong candidates for involvement in DF habituation plasticity before our screen, their previous associations with learning and memory reinforce the idea that these molecules play critical roles in plasticity processes. In support of this idea, we have previously shown that habituation is regulated in a circadian-dependent manner *Randlett et al. (2019)*, and both Melatonin and Estrogen levels fluctuate across the circadian cycle *Alvord et al. (2022); Gandhi et al. (2015); Zhdanova et al. (2001)*, suggesting that either or both of these pathways may act to couple the circadian rhythm with learning performance.

Finally, approximately 2% of the US population use Melatonin as a sleep-aid *Li et al. (2022)*, and a substantial proportion of US women take Estrogen as part of either oral contraceptives or hormone replacement therapy. Therefore, understanding the roles these molecules play in neuroplasticity is a clear public health concern.

Circuit mechanism of DF habituation

Using pERK-based whole brain activity profiling, we first identified that habituation learning is associated with a broad depression of neuronal activity. These data appear consistent with a model for habituation in which plasticity early within the visual pathway acts as an activity bottleneck, perhaps even in the retina. However, our Ca²⁺ imaging experiments identified a diverse range of neuronal *Adaptation Profiles*, including non-adapting and potentiating neurons spread throughout sensory- and motor-related areas of the brain, inconsistent with such a model. Thus, non-habituated signals are transmitted throughout the brain, indicating the presence of parallel processing streams during habituation.

This is more consistent with our previous behavioural analyses of habituation, where we postulated that multiple plasticity loci co-exist, arranged in both parallel and series within the circuit *Randlett et al. (2019)*. Such a model is further supported with brain-wide imaging data for short-term habituation to looming stimuli, where distributed neurons were identified that showed differential rates of habituation *Marquez-Legorreta et al. (2022)*. It is important to point out that Marquez-Legorreta et al. did not observe non-adapting or potentiating neurons in their experiments. This may be due to differences in analysis methods, or could highlight a difference between short-

and long-term habituation circuit mechanisms, the latter of which may rely on more complex circuit mechanisms involving both potentiation and suppression of responses.

While we do not have enough anatomical data to constrain circuit connectivity models that drive DF habituation, here we demonstrate the use of pharmacology, functional imaging and neurotransmitter classifications to constrain our models. Specifically, pharmacology indicated a central role for GABA in habituation, and our functional imaging highlighted a role for distinct classes of neuronal types in the DF circuit, including potentiating neurons (12_M^{Pot}). Initially, this led us to propose a very simple model for habituation, where potentiating neurons are GABAergic and thus progressively inhibit the circuit during learning (Model 1). However, *in silico* co-localization analyses and double transgenic Ca^{2+} imaging identified 12_M^{Pot} neurons to be predominantly non-GABAergic, thereby refuting this simple model. Instead, we propose that the GABAergic neurons in the circuit are characterized by their short burst of activity to the stimulus onset, and that the potentiation of their synapses drives habituation (Model 3, *Figure 8N*). This is a somewhat unexpected model, as studies of long-term synaptic plasticity (e.g. LTP and LTD) have overwhelmingly focused on plasticity at excitatory synapses. Although a functional link to behaviour is less well established, long-term inhibitory synaptic plasticity has been well documented, including inhibitory (i)-LTP and i-LTD *Castillo et al. (2011)*.

A key question then is what underlies the ranges in *Adaptation Profiles* that we see in individual neurons, which include non-adapting, weak-, medium-, and strong-depressing profiles. One possible model is that i-LTP is implemented differentially, which would require a mechanism to drive differential plasticity along different places in the circuit. While feasible, such a mechanism seems somewhat complex. Instead we favor a more parsimonious model in which differential connectivity from inhibitory neurons underlie these dynamics: non-adapting neurons receive little inhibition thus i-LTP has little effect, while strong-depressing neurons receive strong inhibitory connections undergoing i-LTP (Model 2, *Figure 8A*). While this model is certainly incomplete, it provides the initial framework for the circuit-wide mechanisms leading to DF habituation, and testable hypotheses as to the connectivity and functional consequences of manipulations of different neuronal classes.

Conspicuously absent from our models are the 12_M^{Pot} neurons. Since these neurons were increased by both PTX and Melatonin, they might play a complex role in habituation. How they influence the system remains to be seen, but perhaps they act to reinforce activity in weakly habituating neurons. Given their location in the hindbrain they may alternatively directly feed into the reticulospinal system to modulate motor commands. Also absent from our current model are the classes exhibiting an On-response profile (1_{On}^{noA} and 2_{On}^{medD}). These neurons fire at the ramping offset of the stimulus, making it unlikely that they play a role in aspects of acute DF behaviour. However, these neurons exist in both non-adapting and depressing forms suggesting a yet unidentified role in behavioural adaptation to repeated DFs.

Circuit loci of DF habituation

Where in the brain does habituation take place? Our whole-brain MAP-Mapping experiments showed that while DFs activate a very distributed circuit, little activation of the telencephalon or the hypothalamus was seen, indicating that these areas are not involved in the DF response or its habituation. As discussed above, our data is inconsistent with a single-bottleneck model. Instead, plasticity is distributed throughout the circuit. Since PTX inhibits most aspects of habituation learning (*Figure 3Ai*), these all appear to involve GABA motifs. Moreover, the different functional classes of neurons are distributed through sensory- and motor-related areas of the brain, consistent with the notion that habituation plasticity occurs in a very distributed manner. While distributed, there are clear associations between anatomical location and functional neuron type (*Figure 6A-E*), indicating that there is some degree of regional logic to the localization of *Adaptation Profiles*. For example, 5_M^{weakD} and 6_M^{weakD} are the most prevalent in the pretectum, and mostly absent from the tegmentum and posterior hindbrain, whereas 3_L^{medD} and 4_L^{strgD} are numerous in tegmentum and posterior hindbrain, and thus likely occupy more downstream positions in the sensori-motor circuit.

The tectum is one of the largest brain areas in larval zebrafish, and is directly innervated by nearly all retinal ganglion cells *Robles et al. (2014)*. Therefore, the tectum is a prime candidate for implementing DF habituation for anatomical reasons. In further support of this notion, the neurons we have identified as GABAergic and propose to be driving habituation (7_S^{medD} , 8_S^{strgD} , 10_S^{noA} and 11_S^{weakD}) are concentrated in the tectum (*Figure 6C,D*). The tectum contains multiple anatomically distinct types of GABAergic neurons, most of which are locally projecting interneurons (SINs, ITNs, PVINs), although GABAergic projection neurons have been observed with axons projecting to the

anterior hindbrain **Gebhardt et al. (2019); Martin et al. (2022); Nevin et al. (2010); Robles et al. (2011)**. Therefore, we expect that our GABAergic classes correspond to subsets of these GABAergic tectal neurons, which is testable using genetic approaches based on marker co-expression and/or single cell morphometric and transcriptomic analyses.

Beyond the tectum, conspicuous neuronal clustering was observed in the inferior olive and cerebellum, which have been implicated in motor-related learning behaviours in larval zebrafish **Ahrens et al. (2012); Lin et al. (2020); Markov et al. (2021)**. Both structures contained many stimulus-tuned neurons (**Figure 5F**), and non-adapting (1_{On}^{noA} , 9_M^{noA} and 10_S^{noA}), and potentiating (12_M^{pot}) neurons were among the most concentrated in the cerebellum (**Figure 6C,D**). Non-adapting 9_M^{noA} neurons were also prominent in the torus longitudinalis, which also contains high concentrations of on-responding 1_{On}^{noA} , 2_{On}^{medD} neurons. The torus longitudinalis has recently been implicated in the binocular integration of luminance cues **Tesmer et al. (2022)**, and therefore is ideally placed to influence habituation to whole-field stimuli like DFs.

Collectively, our brain-wide imaging data point to a central role for inhibitory neurons in the tectum in habituation, but also clearly implicate other brain areas, and therefore a comprehensive model will need to span many regions of the brain in order to explain the neural and behavioural dynamics underlying habituation learning.

Conclusion

Habituation is the simplest form of learning, yet despite its presumed simplicity a model of how this process is regulated in the vertebrate brain is still emerging. Here we have combined two powerful methods offered by the larval zebrafish model: high-throughput behavioural screening and whole brain functional imaging. By applying these methods to long-term habituation, we identified dozens of pharmacological agents that strongly modulate habituation learning and distinct classes of neurons that are activated by DFs and are modulated during learning. The systematic datasets we generated contain large amounts of additional information that await future validation and integration into a unified model for DF habituation. Nonetheless they yielded a multitude of hypotheses as to the molecular and circuit mechanisms of habituation that can be followed up in future studies.

Our approach validates the utility of virtual anatomical analyses using atlases and pharmacological manipulations to test and constrain neural circuit models in pan-neuronal imaging experiments, for which anatomical and molecular information is often sparse. From these analyses we have arrived at the first iteration of a brain-wide circuit model for long-term dark flash habituation., where distributed plasticity mechanisms mediate the independent adaptation of different components of responses **Randlett et al. (2019)**. The diversity of molecular pathways and functional neuronal types we have identified here are consistent with that view of habituation, and indicate that considerable biological complexity exists that awaits discovery within the "simplest" form of learning.

Methods

Animals

All experiments were performed on larval zebrafish at 5 days post fertilization (dpf), raised at a density of ≈ 1 larvae/ml of E3 media in a 14:10h light/dark cycle at 28-29°C. Wild type zebrafish were of the TLF strain (ZDB-GENO-990623-2). Transgenic larvae used were of the following genotypes: *Tg(elavl3:H2B-GCaMP7f)j^{j90}* **Yang et al. (2021)**, *Tg(elavl3:H2B-GCaMP6s)j^{j5}* **Freeman et al. (2014)**, and *Tg(gad1b:DsRed)nns26* **Satou et al. (2013)**. Zebrafish were housed, cared for, and bred at the Harvard MCB, UPenn CDB, and Lyon PRECI zebrafish facilities. All experiments were done in accordance with relevant approval from local ethical committees at Harvard University, the University of Pennsylvania, and the University of Lyon.

High-throughput screening setup

Larvae were assayed for behaviour in 300-well plates using the apparatus described previously **Randlett et al. (2019)**. Briefly, each well is 8mm in diameter and 6mm deep, yielding a water volume of $\approx 300\mu L$. Behaviour was tracked using a Mikrotron CXP-4 camera, Bitflow CTN-CX4 frame grabber, illuminated with IR LEDs (TSHF5410, digikey.com). Visual stimuli were delivered via a ring of 155 WS2812B RGB LEDs (144LED/M, aliexpress.com). For a dark flash stimulus, the LEDs were turned off for 1s, and then the light intensity was increased linearly to the original brightness over 20s. The optomotor response was induced by illuminating every 8th LED along the top and bottom of the plate, and progressively shifting the illuminated LED down the strip resulting in an approximately sinusoidal stimulus, 5.5

cm peak to peak, translating at 5.5 cm per second. Direction of motion was switched every 30 s, for a total testing period of 1 hour, and performance was scored as the average change in heading direction towards the direction of motion during these 30s epochs. Acoustic tap stimuli were delivered using a Solenoid (ROB-10391, Sparkfun). The behavioural paradigm was designed to be symmetrical such that 1hr worth of stimulation was followed by 1hr worth of rest (*Figure 1B*), allowing us to alternate the view of the camera between two plates using 45-degree incidence hot mirrors (43-958, Edmund Optics) mounted on stepper motors (*Figure 1A*, ROB-09238, Sparkfun), driven by an EasyDriver (ROB-12779, Sparkfun).

Apparatus were controlled using arduino microcontrollers (Teensy 2.0 and 3.2, PJRC) interfaced with custom written software (Multi-Fish-Tracker), available here:

github.com/haesemeyer/MultiTracker.

Behavioural analyses

The behaviour of the fish was tracked online at 28 hz, and 1-second long videos at 560 hz were recorded in response to DF and Acoustic Tap stimuli. Offline tracking on recorded videos was performed in MATLAB (Mathworks) using the script ‘TrackMultiTrackerTiffStacks_ParallelOnFrames.m’, as described previously, to track larval posture *Randlett et al. (2019)*. Tracks were then analyzed using Python. Analysis code available here:

github.com/owenrandlett/lamire_2022.

Responses to DFs and to taps were identified as movement events that had a bend amplitude greater than 3rad and 1rad , respectively. Behavioural fingerprints were created by first calculating the average value for each fish reflecting either the DF response during the specified time period (Naive = DFs 1-5, Training = DFs 6-240, Test = DFs 241-300), or the average response during the entire stimulus period (Acoustic Taps, OMR, Free Swimming). Periods where the tracking data was incomplete were excluded from the analysis. DFs where larvae did not respond were excluded from the behavioural components other than the Probability of Response. The Strictly Standardized Mean Difference was then calculated for each of these average fish values for the drug treated larvae DMSO control (*Figure 1C*). The threshold for determining hit compounds was set at $|SSMD| \geq 2$. These analyses were performed using:

[Analyze_MultiTracker_TwoMeasures.py](https://github.com/owenrandlett/Analyze_MultiTracker_TwoMeasures.py).

Hierarchical clustering (*Figure 1D*, 2A-C) was performed using SciPy *Virtanen et al. (2020)*. Correlations across different behavioural measures (*Figure 2D*) was calculated computing all pairwise comparisons for each behavioural measure in the SSMD fingerprint across the 176 hit compounds.

Further details and code for the analyses used to create the figure panels are in the following notebook: [2022_LamireEtAl_BehavFigs.ipynb](https://github.com/owenrandlett/2022_LamireEtAl_BehavFigs.ipynb). Analyses made use of open-source Python packages, including: NumPy *Harris et al. (2020)*, SciPy *Virtanen et al. (2020)*, matplotlib *Hunter (2007)*, seaborn *Waskom (2021)*, and open-cv *Bradski (2000)*.

Pharmacology

Compounds were prepared as 1000x frozen stock solutions in DMSO. Stock solutions were initially diluted 1:100 in E3, yielding a 10x solution. 30 μL of this solution was then pipetted into the wells, yielding a 1x drug solution in 0.1% DMSO (Sigma). Vehicle treatment followed the same protocol, using pure DMSO. The drug library (Sell-eckchem Bioactive: 2100 FDA-approved/FDA-like small molecules, *Figure 1-source data 1*) was obtained from the UPenn High-Throughput Screening Core. The library concentration was 10mM, and thus all drugs were screened at approximately 10 μM .

For subsequent pharmacological experiments chemicals were obtained from: Picrotoxinin: Sigma, P-8390; Melatonin: Cayman, 14427; Sigma, M5250; Ethinyl Estradiol: Cayman, 10006486; Hexestrol: Sigma, H7753

MAP-Mapping

Immunostaining was performed as previously described *Randlett et al. (2015)*, on wild type zebrafish bleached with 1.5% H_2O_2 , 1% KOH. Confocal stacks were aligned to the Z-Brain atlas coordinates using the computational morphometry toolkit (CMTK, nitrc.org/projects/cmtk/), and calculations of the pairwise differences in pERK/tERK staining were performed as described in, code available here:

github.com/owenrandlett/Z-Brain.

Regional analyses (*Figure 4A-K*(insets), L, M) were performed on regions of the brain as defined by the updated MECE (Mutually Exclusive, Collectively Exhaustive) regional definitions, which unambiguously assign each voxel in the Z-Brain to a single region arranged in a hierarchical ontology (Vorha et al, unpublished) ; available here:

<https://zebrafishatlas.zib.de/lm>

Microscopy

Imaging was performed on 5dpf larvae, mounted tail-free in 2% LMP agarose (Sigma A9414) in E3, using a 20x 1.0NA water dipping objective (Olympus). Volumetric Imaging (*Figure 5*,*Figure 6*, *Figure 8*) was performed at 930 nm on a Bruker Ultima microscope at the , using a resonant scanner resonant scanner over a rectangular region of 1024x512 pixels (0.6 μ m x/y resolution) and piezo objective mount for fast z-scanning. Imaging sessions began by taking an "Anatomy Stack" consisting of 150 slices at 1 μ m z-steps, summed over 128 repeats (imaging time \approx 11 minutes). This served as the reference stack used for alignment to the Z-Brain atlas, and to detect Z-drift in the imaging session (see below). The functional stack consisted of 12 slices separated at 10 μ m steps, thus covering 120 μ m in the brain acquired at 1.98 hz. To image *Tg(elavl3:H2B-GCaMP6s);Tg(gad1b:DsRed)* double transgenic larvae (*Figure 7*), we used a custom built 2-photon microscope *Haesemeyer et al. (2018)*, imaging 512x512 images at (0.98 μ m x/y resolution) at 1.05 hz. The anatomy stack was taken at 2 μ m step sizes for both the green and red channels in the dark. Functional imaging was performed only on the green/GCaMP channel since the red stimulus LED was incompatible with DsRed imaging.

When developing this protocol we determined that substantial shifts of more than a cell-body diameter (5 μ M) in the Z-plane are common during the \approx 1.2 hrs of imaging. We determined this by comparing the sum of the functional image planes during 5 equally sized time epochs (1540 frames per epoch), aligned to the "Anatomy Stack", using "phase_cross_correlation" in the scikit-image library *van der Walt et al. (2014)*. This allowed us to quantify shifts in the imaging plane as shifts in this alignment. These tended to occur within the first hour of imaging, therefore we performed an hour of imaging of this functional stack before beginning the DF stimulation protocol to allow the preparation to settle under imaging conditions. Dark flashes were delivered using a 3mm red LED mounted above the fish, controlled by an Arduino Nano connected to the microscope GPIO board and the Prairie View software to deliver pulses of darkness consisting of 1 sec light off, 20 sec linear ramp back to light on, delivered at 60 second intervals.

Even with this pre-imaging protocol, z-shifts were still observed in a considerable number of fish. Since our habituation-based analysis is focused on how individual neurons change their responses over time, shifts in the z-plane are extremely problematic as they are not correctable post-acquisition and can result in different neurons being imaged at individual voxels. This could easily be confused for changes in functional responses over time during habituation. Therefore, any fish showing a z-drift of greater than 3 μ m was excluded from our analysis. Stable z-positioning was further confirmed by manual inspection of the eigan images in the imaging timecourse using "View registration metrics" in suite2 to confirm that these do not reflect z-drift. Of 56 larvae imaged total, 22 were excluded, leaving 34 included. Larvae were treated with 0.1% DMSO, Picrotoxinin (PTX, 10 μ M), or Melatonin (1 μ M), from approximately 1hr before imaging. These fish were analyzed as a single population (*Figure 5*,*Figure 6*,*Figure 7*) and separately to determine the effects of the treatments (*Figure 8*).

Ca²⁺ imaging analysis

ROIs were identified using suite2p *Pachitariu et al. (2017)* using the parameters outlined in [RunSuite2p_BrukerData_ScreenPaper.py](#) and [RunSuite2p_MartinPhotonData_ScreenPaper.py](#) scripts for the data from the Bruker Ultima microscope (*Figure 5*-*Figure 8*), and custom built 2-photon microscope (*Figure 7D,E*), respectively. These ROIs mostly reflected individual neuronal nuclei/soma. The imaging planes were then aligned to the anatomical stack taken before functional imaging using "phase_cross_correlation" in the scikit-image library *van der Walt et al. (2014)*. For the volumetric data, the anatomical stack was then aligned to the Z-Brain atlas coordinates using CMTK, and ROI coordinates were transformed into Z-Brain coordinates using streamxform in CMTK. These steps were performed using
[??Bruker2p_AnalyzePlanesAndRegister.py](#).

To identify ROIs that were correlated with the stimulus we use a regression-based approach *Miri et al. (2011)*, where we identified ROIs that were correlated with vectors representing the time course of the DF stimuli convolved

with a kernel approximating the slowed H2B-GCaMP time course with respect to neuronal activity. These regressors reflected either the entire 21 second dark flash stimulus, or only the onset of the flash, and either the first 3, last 3, or all 60 flashes (6 regressors in total). To identify neurons correlated to motor output, we took advantage of the plane-based registration statistics calculated by suite2p. Specifically, the “ops[‘corrXY’]” metric, which reflects the correlation of each registered image frame with the reference image. We reasoned that movements would cause image artifacts and distortions that would be reflected as a transient drop in these correlations. Indeed, we confirmed this association by imaging the tail using an infrared camera, and compared the motion index calculated through tail tracking, and that which we calculated based on the motion artifacts, which showed good overall agreement in predicted movement events and average correlation of 0.4, demonstrating that these image-based artifacts can be used as reliable proxies of tail movements (*Figure 5-figure Supplement 1*). Therefore, regressors based on these motion indices were used to identify neurons correlated with motor output.

Images for the functional tuning of individual neurons (*Figure 5E-H*) were computed using the the Hue Saturation Value (HSV) colorscheme, with the maximal correlation value to either regressor mapped to saturation, and the hue value reflecting the linear preference for either regressor. Clustering of functional response types (*Figure 6*) was done by first selecting all those ROIs that showed a correlation of 0.25 or greater with any of the 6 stimulus regressors across all imaged fish. Then among these ROIs we removed any ROIs that did not show a correlation of 0.3 or greater with at least 5 ROIs imaged in a different larvae. This filtered out ROIs that were unique in any individual fish, allowing us to focus on those neuron types that were most consistent across individuals. We then used the Affinity Propagation clustering from scikit-learn *Pedregosa et al. (2011)*, with “affinity” computed as the Pearson product-moment correlation coefficients (corrcoef in NumPy *Harris et al. (2020)*), preference=-9, and damping=0.9.

To generate the final cluster assignments we re-scanned all the ROIs calculating their correlation with the mean-response vectors for each of the identified 12 functional clusters, selecting those with a correlation value of 0.3 or greater, which were then assigned to the cluster with which they had the highest correlation. To determine the cluster assignments for the data from *Tg(Gad1b:DsRed);Tg(elavl3:H2B-GCaMP6s)* double transgenic larvae (*Figure 7D,E*) data were realigned and interpolated to match the frame rate of the clustered data, and assigned to the 12 clusters as above.

To compare the spatial relationships between the neuronal positions of different clusters (*Figure 6E*), and between the clusters and reference brain labels (*Figure 7B,C*), image volumes were cropped to the imaged coordinates (*Figure 5C*), downsampled to isometric 10 μm^3 voxels, and linearized to calculate the Pearson’s correlation coefficient between the image sub-volumes.

Analyses made use of multiple open-source Python packages, including: suite2p *Pachitariu et al. (2017)* NumPy *Harris et al. (2020)*, SciPy *Virtanen et al. (2020)*, scikit-learn *Pedregosa et al. (2011)*, scikit-image *van der Walt et al. (2014)*, numba *Lam et al. (2015)*, matplotlib *Hunter (2007)*, seaborn *Waskom (2021)*, and open-cv *Bradski (2000)*. Details of the analyses used to create the figure panels are in the following notebook:

[2022_LamireEtAl_FunctionalFigs.ipynb](#)

Data and Code Availability

Code for data analysis and for generating the figure panels is available here:

[github.com/owenrandlett/lamire_2022](#)

Data are available here:

[lamire2022.randlettlab.com/](#)

Acknowledgments

We thank the Randlett, Granato and Engert group members for helpful advice regarding the manuscript and work, Gregory Forkin for help in zebrafish husbandry, and the Burgess and Baier groups for sharing anatomical data from the Zebrafish Brain Browser and mapZebrain atlases. This work was supported by funding from the ATIP-Avenir program of the CNRS and Inserm (O.R.), a Fondation Fyssen research grant (O.R.), the IDEX-Impulsion initiative of the University of Lyon (O.R.), the NIH RO1 grants MH109498 (M.G.), NS123887 (M.H.), and the NIH Brain Initiative grants U19NS104653, R24 NS086601, and R43OD024879, as well as Simons Foundation grants SCGB nos. 542973

and 325207 (F.E.)

Author Contributions

Conceptualization: OR, MG
Methodology: OR
Software: OR, MH
Formal Analysis: OR
Investigation: L-AL, OR
Supervision, Resources and Funding Acquisition: FE, MG, OR
Writing – Original Draft Preparation: OR
Writing – Review Editing: MH, FE, MG, LA-L, OR

References

- Ahrens MB, Li JM, Orger MB, Robson DN, Schier AF, Engert F, Portugues R. Brain-wide neuronal dynamics during motor adaptation in zebrafish. *Nature*. 2012 May; 485(7399):471–477.
- Alvord VM, Kantra EJ, Pendergast JS. Estrogens and the circadian system. *Semin Cell Dev Biol*. 2022 Jun; 126:56–65.
- Bailey CH, Chen M. Morphological basis of long-term habituation and sensitization in Aplysia. *Science*. 1983 Apr; 220(4592):91–93.
- Bandara SB, Carty DR, Singh V, Harvey DJ, Vasylieva N, Pressly B, Wulff H, Lein PJ. Susceptibility of larval zebrafish to the seizurogenic activity of GABA type A receptor antagonists. *Neurotoxicology*. 2020 Jan; 76:220–234.
- Baraban SC, Taylor MR, Castro PA, Baier H. Pentylenetetrazole induced changes in zebrafish behavior, neural activity and c-fos expression. *Neuroscience*. 2005; 131(3):759–768.
- Bradski G. The openCV library. *Dr Dobb's Journal: Software Tools for the Professional Programmer*. 2000; 25(11):120–123.
- Bruni G, Rennekamp AJ, Velenich A, McCarroll M, Gendelev L, Fertsch E, Taylor J, Lakhani P, Lensen D, Evron T, Lorello PJ, Huang XP, Kolczewski S, Carey G, Calderone BJ, Prinsen E, Roth BL, Keiser MJ, Peterson RT, Kokel D. Zebrafish behavioral profiling identifies multitarget antipsychotic-like compounds. *Nat Chem Biol*. 2016 Jul; 12(7):559–566.
- Burgess HA, Granato M. Modulation of locomotor activity in larval zebrafish during light adaptation. *J Exp Biol*. 2007 Jul; 210(Pt 14):2526–2539.
- Castillo PE, Chiu CQ, Carroll RC. Long-term plasticity at inhibitory synapses. *Curr Opin Neurobiol*. 2011 Apr; 21(2):328–338.
- Chen X, Engert F. Navigational strategies underlying phototaxis in larval zebrafish. *Front Syst Neurosci*. 2014 Mar; 8:39.
- Cheng XP, Sun H, Ye ZY, Zhou JN. Melatonin modulates the GABAergic response in cultured rat hippocampal neurons. *J Pharmacol Sci*. 2012 May; 119(2):177–185.
- Cooke SF, Komorowski RW, Kaplan ES, Gavornik JP, Bear MF. Visual recognition memory, manifested as long-term habituation, requires synaptic plasticity in V1. *Nat Neurosci*. 2015 Feb; 18(2):262–271.
- Cooke S, Ramaswami M. Ignoring the Innocuous: The Neural Mechanisms of Habituation. In: *The Cognitive Neurosciences: 6th Edition* MIT Press; 2020.p. 197.
- Das S, Sadanandappa MK, Dervan A, Larkin A, Lee JA, Sudhakaran IP, Priya R, Heidari R, Holohan EE, Pimentel A, Gandhi A, Ito K, Sanyal S, Wang JW, Rodrigues V, Ramaswami M. Plasticity of local GABAergic interneurons drives olfactory habituation. *Proc Natl Acad Sci U S A*. 2011 Sep; 108(36):E646–54.
- Dillon TS, Samuel Dillon T, Fox LC, Han C, Linster C. 17β -estradiol enhances memory duration in the main olfactory bulb in CD-1 mice; 2013.
- Dunn TW, Mu Y, Narayan S, Randlett O, Naumann EA, Yang CT, Schier AF, Freeman J, Engert F, Ahrens MB. Brain-wide mapping of neural activity controlling zebrafish exploratory locomotion. *Elife*. 2016 Mar; 5:e12741.
- El-Sherif Y, Tesoriero J, Hogan MV, Wierszko A. Melatonin regulates neuronal plasticity in the hippocampus. *J Neurosci Res*. 2003; 72(4):454–460.

Förster D, Helmbrecht TO, Mearns DS, Jordan L, Mokayes N, Baier H. Retinotectal circuitry of larval zebrafish is adapted to detection and pursuit of prey; 2020.

Freeman J, Vladimirov N, Kawashima T, Mu Y, Sofroniew NJ, Bennett DV, Rosen J, Yang CT, Looger LL, Ahrens MB. Mapping brain activity at scale with cluster computing. *Nat Methods*. 2014 Sep; 11(9):941–950.

Gandhi AV, Mosser EA, Oikonomou G, Prober DA. Melatonin is required for the circadian regulation of sleep. *Neuron*. 2015 Mar; 85(6):1193–1199.

Gebhardt C, Auer TO, Henriques PM, Rajan G, Duroure K, Bianco IH, Del Bene F. An interhemispheric neural circuit allowing binocular integration in the optic tectum. *Nat Commun*. 2019 Nov; 10(1):5471.

Glanzman DL. Habituation in Aplysia: the Cheshire cat of neurobiology. *Neurobiol Learn Mem*. 2009 Sep; 92(2):147–154.

Gupta T, Marquart GD, Horstick EJ, Tabor KM, Pajevic S, Burgess HA. Morphometric analysis and neuroanatomical mapping of the zebrafish brain. *Methods*. 2018 Nov; 150:49–62.

Haesemeyer M, Robson DN, Li JM, Schier AF, Engert F. A Brain-wide Circuit Model of Heat-Evoked Swimming Behavior in Larval Zebrafish. *Neuron*. 2018 May; 98(4):817–831.e6.

Harris CR, Millman KJ, van der Walt SJ, Gommers R, Virtanen P, Cournapeau D, Wieser E, Taylor J, Berg S, Smith NJ, Kern R, Picus M, Hoyer S, van Kerkwijk MH, Brett M, Haldane A, Del Río JF, Wiebe M, Peterson P, Gérard-Marchant P, et al. Array programming with NumPy. *Nature*. 2020 Sep; 585(7825):357–362.

Hunter. Matplotlib: A 2D Graphics Environment. . 2007 May; 9:90–95.

Jilg A, Bechstein P, Saade A, Dick M, Li TX, Tosini G, Rami A, Zemmar A, Stehle JH. Melatonin modulates daytime-dependent synaptic plasticity and learning efficiency. *J Pineal Res*. 2019 Apr; 66(3):e12553.

Kaplan ES, Cooke SF, Komorowski RW, Chubykin AA, Thomazeau A, Khibnik LA, Gavornik JP, Bear MF. Contrasting roles for parvalbumin-expressing inhibitory neurons in two forms of adult visual cortical plasticity. *Elife*. 2016 Mar; 5.

Kunst M, Laurell E, Mokayes N, Kramer A, Kubo F, Fernandes AM, Förster D, Dal Maschio M, Baier H. A Cellular-Resolution Atlas of the Larval Zebrafish Brain; 2018.

Lam SK, Pitrou A, Seibert S. Numba: a LLVM-based Python JIT compiler. In: *Proceedings of the Second Workshop on the LLVM Compiler Infrastructure in HPC* No. Article 7 in LLVM '15, New York, NY, USA: Association for Computing Machinery; 2015. p. 1–6.

Li J, Somers VK, Xu H, Lopez-Jimenez F, Covassin N. Trends in Use of Melatonin Supplements Among US Adults, 1999–2018. *JAMA*. 2022 Feb; 327(5):483–485.

Lin Q, Manley J, Helmreich M, Schlumm F, Li JM, Robson DN, Engert F, Schier A, Nöbauer T, Vaziri A. Cerebellar Neurodynamics Predict Decision Timing and Outcome on the Single-Trial Level. *Cell*. 2020 Jan; 0(0).

Luine VN, Richards ST, Wu VY, Beck KD. Estradiol enhances learning and memory in a spatial memory task and effects levels of monoaminergic neurotransmitters. *Horm Behav*. 1998 Oct; 34(2):149–162.

Markov DA, Petrucco L, Kist AM, Portugues R. A cerebellar internal model calibrates a feedback controller involved in sensorimotor control. *Nat Commun*. 2021 Nov; 12(1):6694.

Marquart GD, Tabor KM, Horstick EJ, Brown M, Geoca AK, Polys NF, Nogare DD, Burgess HA. High-precision registration between zebrafish brain atlases using symmetric diffeomorphic normalization. *Gigascience*. 2017 Aug; 6(8):1–15.

Marquez-Legorreta E, Constantin L, Piber M, Favre-Bulle IA, Taylor MA, Blevins AS, Giacometto J, Bassett DS, Vanwalleghem GC, Scott EK. Brain-wide visual habituation networks in wild type and fmr1 zebrafish. *Nat Commun*. 2022; 13(1):1–19.

Martin A, Babbitt A, Pickens AG, Pickett BE, Hill JT, Suli A. Single-Cell RNA Sequencing Characterizes the Molecular Heterogeneity of the Larval Zebrafish Optic Tectum. *Front Mol Neurosci*. 2022 Feb; 15:818007.

Maugars G, Nourizadeh-Lillabadi R, Weltzien FA, New Insights Into the Evolutionary History of Melatonin Receptors in Vertebrates, With Particular Focus on Teleosts; 2020.

McDiarmid TA, Belmadani M, Liang J, Meili F, Mathews EA, Mullen GP, Hendi A, Wong WR, Rand JB, Mizumoto K, Haas K, Pavlidis P, Rankin CH. Systematic phenomics analysis of autism-associated genes reveals parallel networks underlying reversible impairments in habituation. *Proc Natl Acad Sci U S A*. 2019 Nov; .

McDiarmid TA, Yu AJ, Rankin CH. Habituation Is More Than Learning to Ignore: Multiple Mechanisms Serve to Facilitate Shifts in Behavioral Strategy. *Bioessays*. 2019 Aug; 8:1900077.

- Miri A**, Daie K, Burdine RD, Aksay E, Tank DW. Regression-based identification of behavior-encoding neurons during large-scale optical imaging of neural activity at cellular resolution. *J Neurophysiol*. 2011 Feb; 105(2):964–980.
- Nelson JC**, Shoenhard HM, Granato M. Pharmacogenetic and whole-brain activity analyses uncover integration of distinct molecular and circuit programs that drive learning; 2022.
- Nevin LM**, Robles E, Baier H, Scott EK, Focusing on optic tectum circuitry through the lens of genetics; 2010.
- Niles LP**, Pickering DS, Arciszewski MA. Effects of chronic melatonin administration on GABA and diazepam binding in rat brain. *J Neural Transm*. 1987; 70(1-2):117–124.
- Nilsson S**, Gustafsson JA. Biological role of estrogen and estrogen receptors. *Crit Rev Biochem Mol Biol*. 2002; 37(1):1–28.
- Pachitariu M**, Stringer C, Dipoppa M, Schröder S, Rossi LF, Dalgleish H, Carandini M, Harris KD. Suite2p: beyond 10,000 neurons with standard two-photon microscopy; 2017.
- Paranjpe P**, Rodrigues V, VijayRaghavan K, Ramaswami M. Gustatory habituation in *Drosophila* relies on rutabaga (adenylate cyclase)-dependent plasticity of GABAergic inhibitory neurons. *Learn Mem*. 2012 Nov; 19(12):627–635.
- Pedregosa F**, Varoquaux G, Gramfort A, Michel V, Thirion B, Grisel O, Blondel M, Prettenhofer P, Weiss R, Dubourg V, Others. Scikit-learn: Machine learning in Python. *the Journal of machine Learning research*. 2011; 12:2825–2830.
- Ramaswami M**. Network Plasticity in Adaptive Filtering and Behavioral Habituation. *Neuron*. 2014 Jun; 82(6):1216–1229.
- Randlett O**, Haesemeyer M, Forkin G, Shoenhard H, Schier AF, Engert F, Granato M. Distributed Plasticity Drives Visual Habituation Learning in Larval Zebrafish. *Curr Biol*. 2019 Apr; 29(8):1337–1345.e4.
- Randlett O**, Wee CL, Naumann EA, Nnaemeka O, Schoppik D, Fitzgerald JE, Portugues R, Lacoste AMB, Riegler C, Engert F, Schier AF. Whole-brain activity mapping onto a zebrafish brain atlas. *Nat Methods*. 2015 Sep; 12(11):1039–1046.
- Rankin CH**, Abrams T, Barry RJ, Bhatnagar S, Clayton DF, Colombo J, Coppola G, Geyer MA, Glanzman DL, Marsland S, McSweeney FK, Wilson DA, Wu CF, Thompson RF. Habituation revisited: an updated and revised description of the behavioral characteristics of habituation. *Neurobiol Learn Mem*. 2009 Sep; 92(2):135–138.
- Rawashdeh O**, de Borsetti NH, Roman G, Cahill GM. Melatonin suppresses nighttime memory formation in zebrafish. *Science*. 2007 Nov; 318(5853):1144–1146.
- Rihel J**, Prober DA, Arvanites A, Lam K, Zimmerman S, Jang S, Haggarty SJ, Kokel D, Rubin LL, Peterson RT, Schier AF. Zebrafish behavioral profiling links drugs to biological targets and rest/wake regulation. *Science*. 2010 Jan; 327(5963):348–351.
- Robles E**, Laurell E, Baier H. The retinal projectome reveals brain-area-specific visual representations generated by ganglion cell diversity. *Curr Biol*. 2014 Sep; 24(18):2085–2096.
- Robles E**, Smith SJ, Baier H. Characterization of genetically targeted neuron types in the zebrafish optic tectum. *Front Neural Circuits*. 2011 Feb; 5:1.
- Rose JK**, Kaun KR, Chen SH, Rankin CH. GLR-1, a non-NMDA glutamate receptor homolog, is critical for long-term memory in *Caenorhabditis elegans*. *J Neurosci*. 2003 Oct; 23(29):9595–9599.
- Satou C**, Kimura Y, Hirata H, Suster ML, Kawakami K, Higashijima SI. Transgenic tools to characterize neuronal properties of discrete populations of zebrafish neurons. *Development*. 2013 Sep; 140(18):3927–3931.
- Shainer I**, Kuehn E, Laurell E, Al Kassar M, Mokayes N, Sherman S, Larsch J, Kunst M, Baier H. A single-cell resolution gene expression atlas of the larval zebrafish brain; 2022.
- Tabor KM**, Marquart GD, Hurt C, Smith TS, Geoca AK, Bhandiwad AA, Subedi A, Sinclair JL, Polys NF, Burgess HA. Brain-wide cellular resolution imaging of Cre transgenic zebrafish lines for functional circuit-mapping; 2018.
- Tesmer AL**, Fields NP, Robles E. Input from torus longitudinalis drives binocularity and spatial summation in zebrafish optic tectum. *BMC Biol*. 2022 Jan; 20(1):24.
- Trisal S**, Aranha M, Chodankar A, VijayRaghavan K, Ramaswami M. A DROSOPHILA CIRCUIT FOR HABITUATION OVERRIDE. *J Neurosci*. 2022 Mar; .
- Virtanen P**, Gommers R, Oliphant TE, Haberland M, Reddy T, Cournapeau D, Burovski E, Peterson P, Weckesser W, Bright J, van der Walt SJ, Brett M, Wilson J, Millman KJ, Mayorov N, Nelson ARJ, Jones E, Kern R, Larson E, Carey CJ, et al. SciPy 1.0: fundamental algorithms for scientific computing in Python. *Nat Methods*. 2020 Mar; 17(3):261–272.

van der Walt S, Schönberger JL, Nunez-Iglesias J, Boulogne F, Warner JD, Yager N, Gouillart E, Yu T, scikit-image contributors. scikit-image: image processing in Python. PeerJ. 2014 Jun; 2:e453.

Waskom M. seaborn: statistical data visualization. J Open Source Softw. 2021 Apr; 6(60):3021.

Yang E, Zwart MF, Rubinov M, James B, Wei Z, Narayan S, Vladimirov N, Mensh BD, Fitzgerald JE, Ahrens MB. A brainstem integrator for self-localization and positional homeostasis; 2021.

Zhdanova IV, Wang SY, Leclair OU, Danilova NP. Interactive report. Brain Res. 2001; 903:263–268.

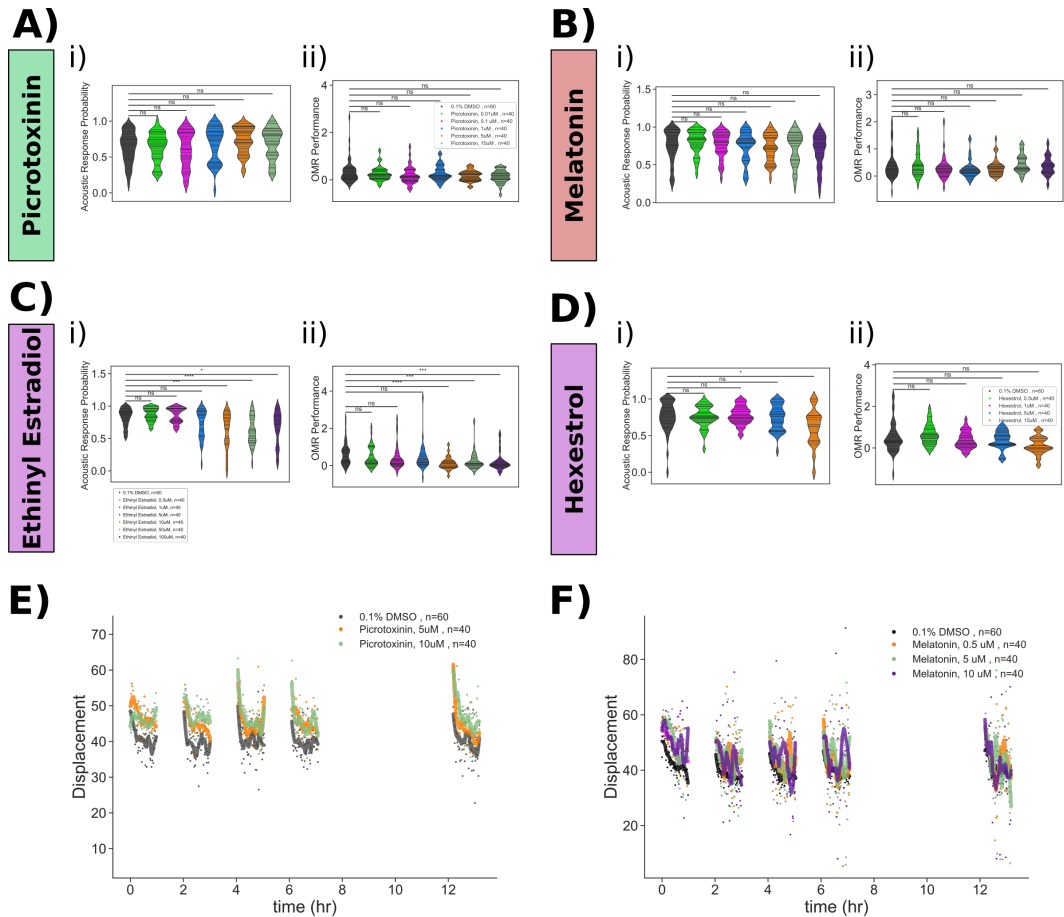


Figure 3—figure supplement 1. Pharmacological manipulation of control behaviours and response displacement during habituation.

Dose response studies for **A) Picrotoxinin**, **B) Melatonin**, **C) Ethynodiol Estradiol** and **D) Hexestrol**. Displayed for each treatment are: i) Violin plots for the dose response data, showing the probability of response to 30 acoustic tap stimuli. Horizontal lines = individual fish. ii) Violin plots for the dose response data OMR performance. Horizontal lines = individual fish. Statistical tests: Mann Whitney with bonferroni correction, ns=not significant; $p \leq **** = 1 \times 10^{-4}$; *** = 1×10^{-3} ; ** = 1×10^{-2} ; * = 0.05.

E) Treatment with Picrotoxinin inhibits the decreases in movement displacement during habituation training.

F) Treatment with Melatonin inhibits the decreases in movement displacement during habituation training. Each dot is the mean response of the population to one flash. Lines are smoothed in time with a Savgolay Filter (window = 15 stimuli, order=2).

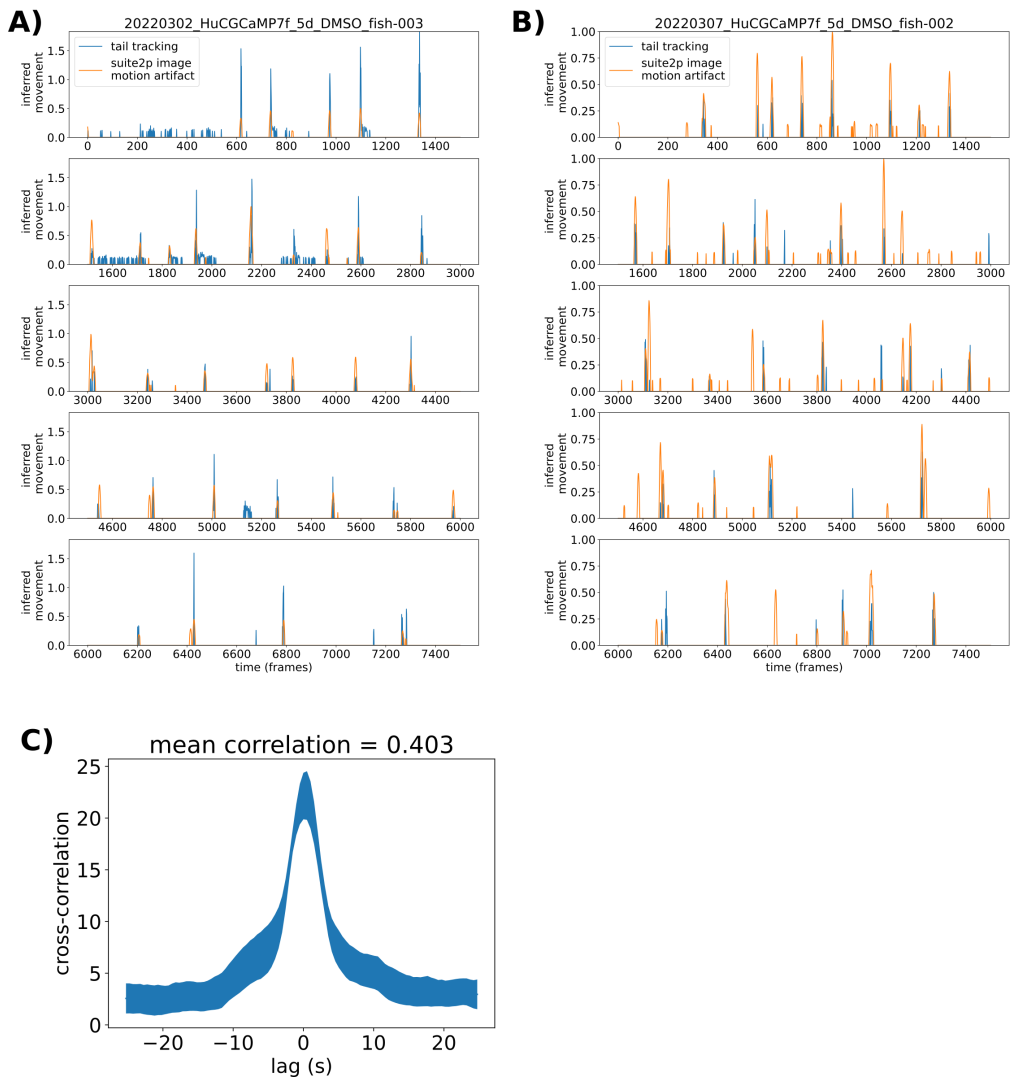


Figure 5—figure supplement 1. Validation of motion analysis based on image artifacts during 2-photon imaging.
A) Motion indexes as calculated based on tail tracking (blue) and based on decreases in the correlation between individual frames and the reference frame used for motion alignment (orange) across the entire imaging experiment (65 minutes).
B) Same analysis as (A), for a different larva.
C) Cross-correlation plot comparing the two motion index vectors. Mean across 6 larvae, and line thickness = standard error.

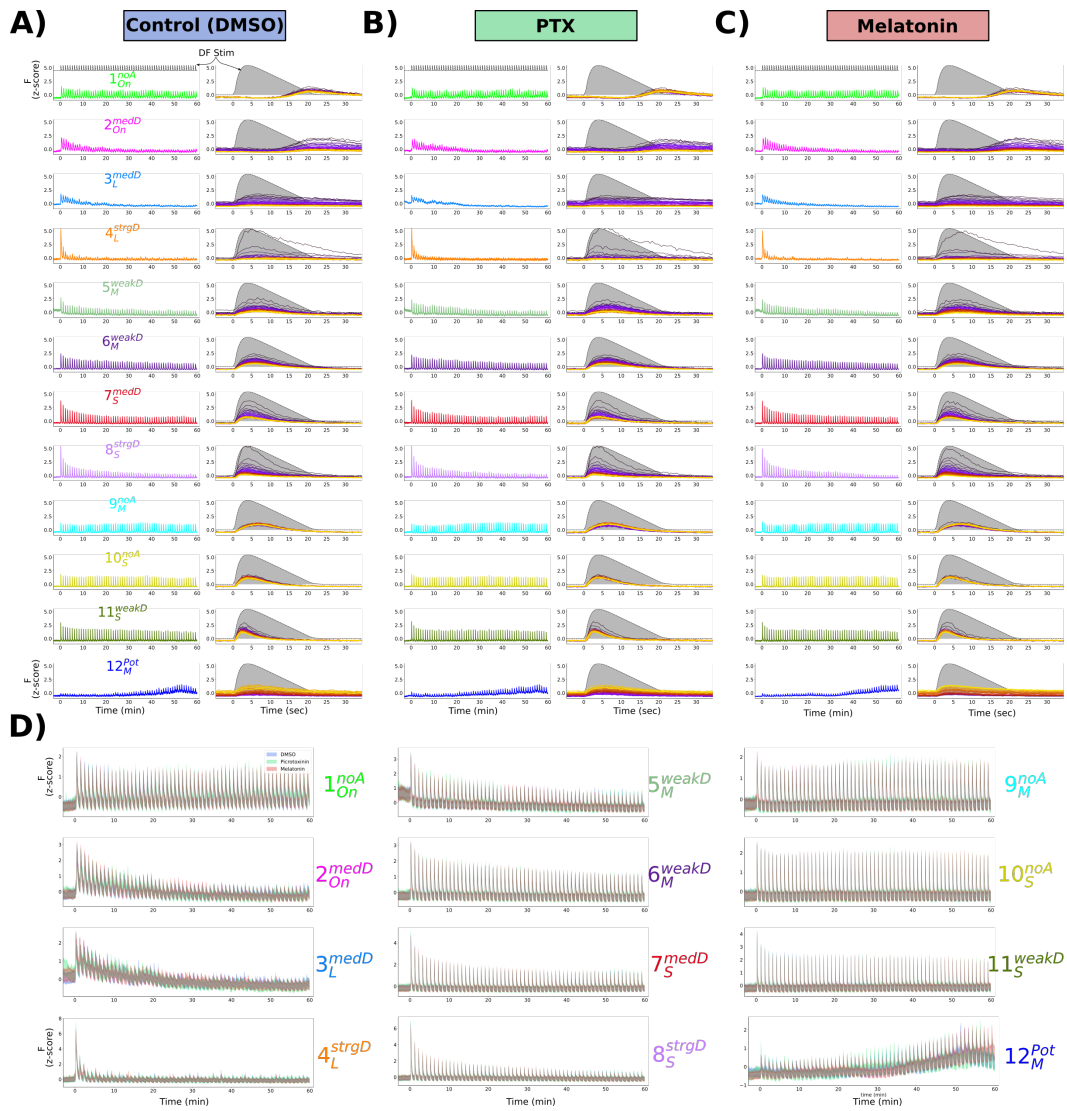


Figure 8—figure supplement 1. Mean response of functionally identified clusters after different pharmacological treatments. **A-C)** Average z-scored fluorescence each functional cluster plotted for the whole experiment (left column), and centered on each DF stimulus (right column), demonstrating the differences in both adaptation and *Response Shape* for each cluster after treatment with **(A)** 0.1% DMSO vehicle control, **(B)** Picrotoxinin (10 μ M), or **(C)** Melatonin (1 μ M). **D)** Same data as A-C, plotted together for each treatment group.